A magnetic survey over part of the stublick fault system and its geophysical interpretation

Smith, R. M.

A MAGNETIC SURVEY OVER PART OF THE STUBLICK FAULT SYSTEM AND ITS GEOPHYSICAL INTERPRETATION

By

R. M. Smith

For the Degree of M. Sc.
in the University of Durham

December 1962

CONTENTS

ILLUSTRATIONS

FIGURE

CHAPTER I

Introduction and Geology

(a). Introduction.

A magnetic survey and its interpretation of part of the Stublick Fault system of Northern England is described in this thesis. The investigation was originally suggested by Dr.M.H.P.Bott in 1958, after he and Dr.D.Masson-Smith had proved a small anomaly existed near Haltwhistle (Bott and Masson-Smith, 1957). However, in 1958 the writer carried out a preliminary magnetic survey in this region with the intention of presenting a small dissertation for the B.Sc. degree. During this work considerably greater anomalies than had hitherto been realised were discovered across the Stublick Fault. The major part of the field work was done during September and October 1959, using a Watt's vertical field magnetometer borrowed from the Geology Department of the Durham Colleges. The field work was completed during April 1960.

On both occasions the writer worked by himself but in 1958 he did not have the use of a motor-car. The area concerned covers about four by five miles and lies roughly two miles south of Haltwhistle (see figure 1). The area is readily accessible by road, except in those tracts covered by heather and rough grass moorland.

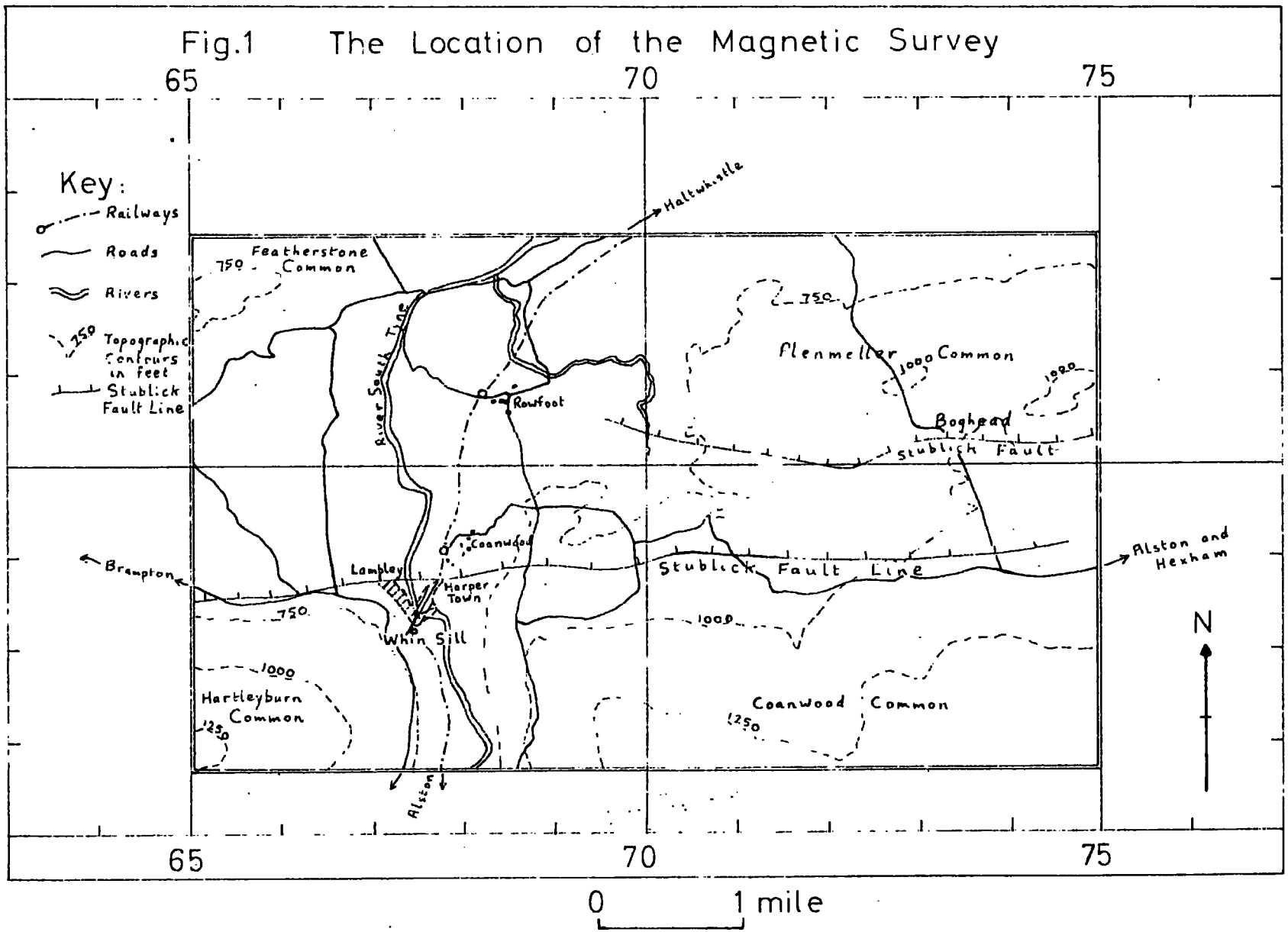
Fig.1 The Location of the Magnetic Survey
65
70
75
60
Key:
Railways
Roads
Rivers
750 Topographic Contours in feet
Stublick Fault Line
Haltwhistle
Featherstone Common
750
River South Tyne
Rowfoot
Plenmeller Common
1000
1000
Boghead
Stublick Fault
Brampton
Lambley
Coanwood
Harper Town
Whin Sill
Stublick Fault Line
Alston and Hexham
N
750
1000
Hartleyburn Common
1250
Coanwood Common
1250
Alston
0
1 mile

(b). Stratigraphy.

A geological map of the Haltwhistle area is shown in figure 2. Only those rocks belonging to the Carboniferous period can be seen at the surface within the investigated area. A classification of the Carboniferous is given in Table 1. The pre-Carboniferous basement rocks are thought to lie at 1500 to 2000 feet below the surface south of the Stublick Fault (Trotter and Hollingworth, 1932). In the Crook borehole (Woolacott, 1923) pre-Devonian rocks were found which were highly folded and cleaved slates showing slight metamorphic effects. Other occurrences of pre-Carboniferous basement rocks are in the Cross Fell and Teesdale inliers. They are unconformably overlain by the basal conglomerates of the Carboniferous.

The thickness of the Carboniferous is thought to change considerably across the Stublick Fault. This is based on evidence several miles from the Stublick Fault. For instance in the Bewcastle Fells north of the fault the Lower Carboniferous, consisting of limestones and interbedded shales and sandstones of the Tuedian and Lower Bernician series, attains a thickness of five to six thousand feet (Trotter and Hollingworth, 1932). In the Cross Fell inlier, south of the Stublick Fault, these rocks are absent, and the Upper Bernician rests directly upon the basal conglomerate. In both areas the Upper Bernician consists of Lower, Middle, and Upper Limestone Groups (see Table 1). Evidence for a change in thickness in the Upper Bernician is found within a mile or two of the fault (Haydon Bridge - Dunham, 1948). The only other clear evidence that the change in thickness corresponds within a zone between the fault and about two miles to the north comes from a gravity survey (Bott and Masson-Smith, 1957). The rocks of the Upper Bernician show rhythmic cycles of deposition, which represent

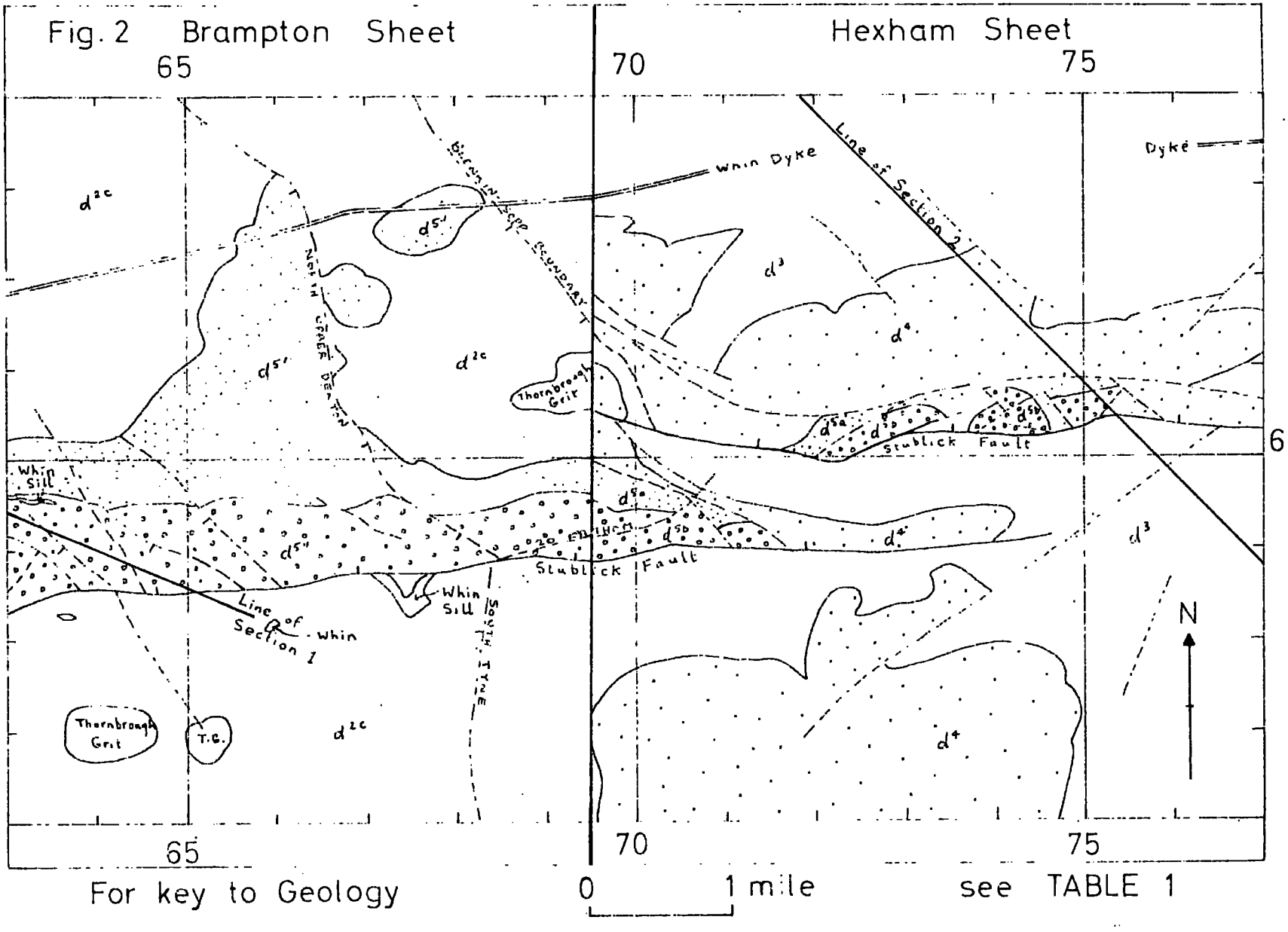
Fig. 2 Brampton Sheet
Hexham Sheet
65
70
75
60
Whin Dyke
Dyke
Line of Section 2
Thornbrough Grit
Stublick Fault
Whin Sill
Line of Section 1
T.C.
N
0
1 mile
For key to Geology
see TABLE 1

TABLE 1 (from the Brampton Sheet and Trotter & Hollingworth, 1932)

			North	South
C.M.		d^{5b} = d^{5b}	Middle C. M.	Craignook, 3/4, & Well Syke Seams Cannel, Slag, & Low Main Seams
		d^{5a} = d^{5a}	Lower C. M.	two seams
Upper Bernician		d^{2c} ($\approx d^{3}$ and d^{4})	Upper Limestone Group	Upper and Lower Felltop Lst. Thornborough Grit, Lst., & Coal Corbridge Lst. Upper, Mid., Lwr. Oakwood Lst. & Coal Firestone Sill Little Lst. & Coal Great Lst.
		d^{2b}	Middle Limestone Group	4 Fath., 3 Yd., & 5 Yd. Lst. & Coal Scar Lst. & Coal Tyne-Bottom, Jew, & Greengate Well Lst. Bankhouses = Smiddy Lst.
		d^{2a}	Lower Limestone Group	Lwr. Tipalt Lst. Melmerby Scar Lst. (inc. Denton Mill Lst.) Naworth Lst.
Lwr. Bern.		$d^{1c'}$	Birdoswald Limestone Group	Basement
		d^{1c}	Craighill Sandstone Group	Conglomerate
Tuedian		d^{1b}	Fell Sandstone Group	
		d^{1a}	Cementstones Group	

deltaic conditions and are charactaristic of the Yoredale facies. A typical cycle would be shale or mudstone, sandstone or grit, coal, and limestone. Outliers of Lower and Middle Coal Measures, to be found north of the Stublick Fault, rest directly upon the Upper Limestone Group. The highest beds of the Carboniferous within the investigated area are the Upper Craignook series of the Middle Coal Measures : these are exposed in a stream section in the Cristowell Burn about one mile east of — — — — — — — — —

westerly throw, separates the two Coal Measure outliers. Trotter and Hollingworth (1932, p.9) regard the trough faults to be mostly tear faults. Small anticlines and synclines are associated with these but the greatest folding occurs in the Bewcastle Anticline in the north-west. Further reference will be made to faulting and folding in the geological history section below.

(d). Igneous Activity.

The only exposed igneous rocks in the area belong to the Great Whin Sill Group. These consist of a series of intruded transgressive sheets, and the Haltwhistle Dyke. The latter, related to the Whin Sill, is part of the St. Oswald's Chapel Dyke-Echelon (Holmes and Harwood, 1928).

Petrologically the Whin Sill is usually a quartz-dolerite, but it can vary in texture from a basalt to a gabbro. In this area it is primarily a medium to finely crystalline quartz-dolerite with only minor coarser variations. The colour is dark grey and the rock is speckled in appearance. The average mineral composition and volume percentages of specimens taken from two sites in Northern England are given in Table 2 (Tomkeieff, 1929).

The Whin Sill lies at a depth of over 2000 feet north of the Stublick Fault (Geological Survey map, Brampton Sheet). It dips south south-eastwards south of the fault [redacted]. Its depth is not known in the area near to Boghead in the east, bordering the en-echelon fault. It is only exposed in the South Tyne valley in the west, near Harper Town, where it is sharply truncated by the fault and quarries in it reveal a thickness of 80 to 100 feet. Here it lies in the Upper Limestone Group, between the Little Limestone and the Firestone

TABLE 2 (from Tomkeieff, 1929)

Mineral composition of a coarse grained variety of Whin Sill (percentage by volume).

	Crook Bore	High Force	Average Volume	Average Weight
Felspar	41.35	41.18	41.27	37.21
Micropegmatite	17.71	18.23	17.97	15.86
Quartz	2.80	2.76	2.78	2.47
Pyroxene	20.25	19.35	19.80	22.22
Hornblende, chlorite, etc.	10.54	9.72	10.13	9.20
Iron ore	7.19	8.68	7.93	12.82
Iron pyrites	0.16	0.08	0.12	0.22

Fig. 3

Hexham Sheet 19

Section 2

NW SE

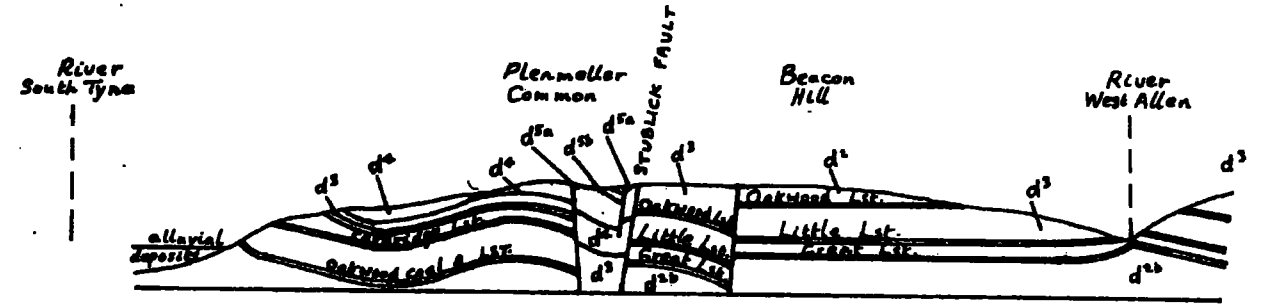

Brampton Sheet 18

Section 1

NW SE

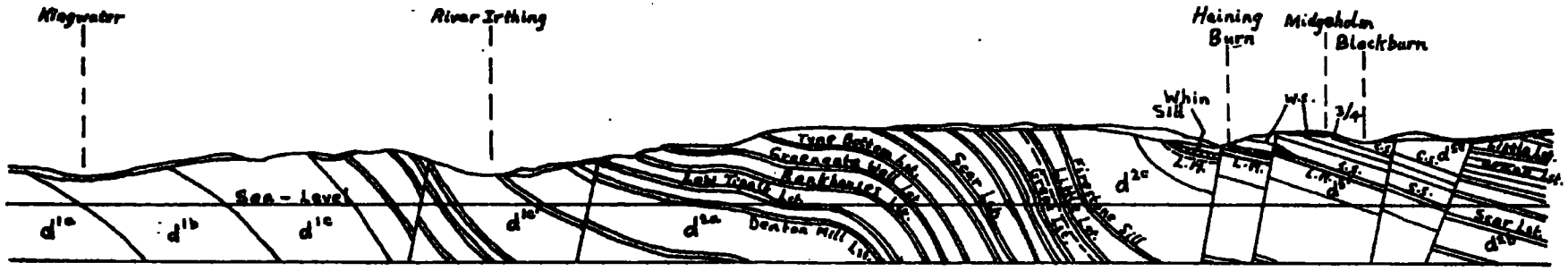

vertical scale 0 ..... 2000 ft.

horizontal scale 0 ——— 1 mile

Sill. Vertical columnar jointing occurs, and there are indications that the Whin Sill may be lenticular (Trotter and Hollingworth, 1932, p.118). Apart from this single exposure its presence in the area has been proved in some borings. South of the Stublick Fault the Whin Sill has the form of lenses or phacolites at various horizons, but north of it continuous sheets and few horizon changes are more usual (Trotter and Hollingworth, 1932, p.113). Further reference will be made to these features in Chapter V. Trotter and Hollingworth (1932, p.119) refer to a dyke having been reported in the coal workings near Cristowell Burn along the line of the Stublick Fault: this may be related to the sill.

The igneous intrusions coincided with a period of strong east north-east compression, limiting their westward extension (Trotter and Hollingworth, 1928). The relation of the sills to the folds and faults strongly suggests an early Hercynian or Carboniferous-Permian interval age (Trotter and Hollingworth, 1932). Further independent evidence supporting this conclusion is the occurrence of a pebble, characteristic of the Whin Sill rocks, in the brockrams of the Eden valley (Holmes and Harwood, 1928), and on the Alston Block mineral veins clearly cut the Whin Sill. Heavy detrital mineral grains from the Whin Sill have also been found in the Permian Yellow Sands (Holmes and Harwood, 1928) showing that the Whin Sill preceded the mineralisation of Northern England.

(e). Geological History.

The sequence of geological events, between Caledonian movements and the Tertiary era, is described in this section.

In the Caledonian period there was east north-east folding of the Lower Palaeozoic rocks, with a development of cleavages (Shotton, 1935), from a probable regional north-west /

south-east compression. Rocks of the Devonian period are probably not present in the region. It is supposed that a marginal hinge-line was initiated in the early Carboniferous resulting in a progressive downwarping of the area north of it. Sedimentation probably began earlier in the Northumbrian Trough than on the Alston Block where deposition did not begin until Lower Limestone times. Following the Coal Measures there were major regional movements heralding the Hercynian tectonic period. The Alston Block, behaving as a rigid unit, was pushed bodily northwards towards the Southern Uplands (Trotter and Hollingworth, 1928). The sediments in the trough were buckled into the Bewcastle Anticline, together with the formation of Master Joints (Dunham, 1948). The following tectonic events are less certain. Trotter and Hollingworth (1928) believe that the Alston Block was then depressed relative to the trough with north north-west and east-west normal faulting along the Stublick Fault line. Here, the throw (southwards) was 250 feet (Versey, 1927), and at the Upper Denton Fault, 150 feet. The Whin Sill and related dykes were then intruded into the Carboniferous rocks. Figure 4 shows Versey's interpretation (1927) of the sudden downward change in horizon of the sill across the Stublick and Denton Faults. In other words, according to Trotter and Hollingworth, to explain this horizon change the Alston Block must have subsided before the intrusions. The Hercynian period ended with a torsional movement of the Block resulting in a gentle doming with the formation of vein fissures (Dunham, 1948). The final major faulting along the Stublick Fault line, displacing Permian and Triassic beds elsewhere, may have taken place in two stages (Trotter and Hollingworth, 1932) and it is possible that the second stage, resulting in the elevation and tilting of the Block to the east, is of Tertiary age (Trotter, 1929).

Fig. 4

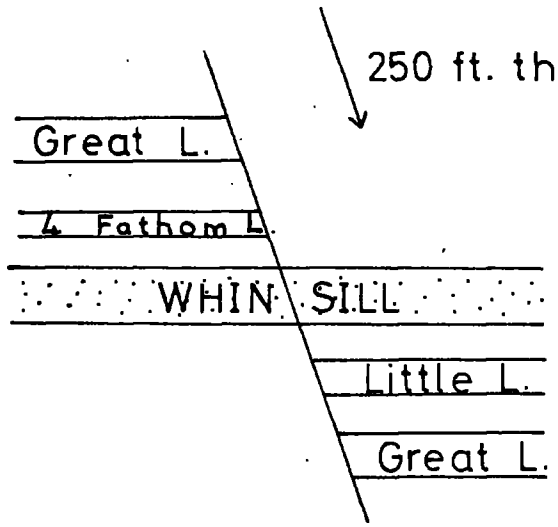

Whin Sill intruded across
the Stublick Fault (Versey)

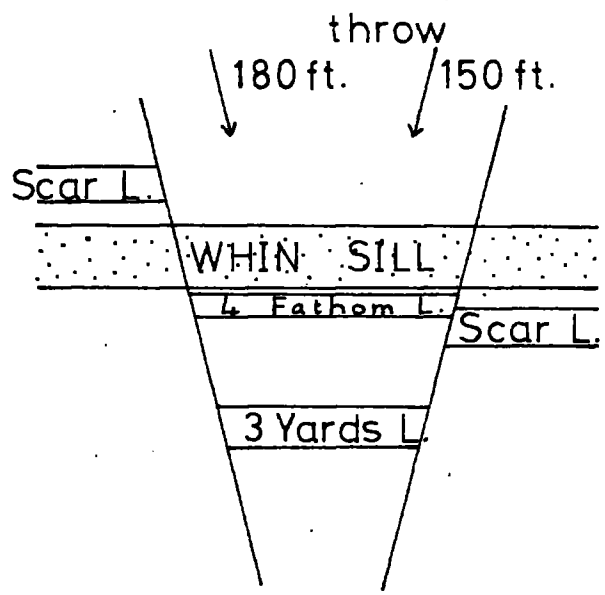

Whin Sill intruded across
the Denton Faults (Versey)

Further knowledge of the region's structure, with particular emphasis on the Stublick Fault and the Whin Sill igneous rocks, could possibly be obtained by conducting a detailed magnetic survey in the vicinity of the Stublick Fault near Haltwhistle. The field work of this survey, together with the routine reduction procedures, forms the basis of the following chapter.

CHAPTER II

Field Work and Reductions of Observations

The main part of the magnetic survey was carried out in ideal weather conditions during a four-week period in September and October, 1959. The survey was completed during a week of field work in April, 1960. Out of 783 observations, 687 were new magnetic stations, of which 22 were bases and auxiliary bases, 4 were outside the limits of the area, and 7 were rejected as unreliable.

A Watt's vertical field magnetometer was used for the surveys. It was calibrated in the field at the beginning and end of the main survey using the auxiliary magnets supplied by the makers. The instrument was also calibrated using Helmholtz coils belonging to Birmingham University, but the values obtained appeared to be unreliable owing to a considerable inconsistency of the results, and were discarded. Further tests using the same auxiliary magnets as were used previously were completed a few weeks later and it was found that these results were consistent with the earlier magnet calibration. The factor adopted was 30.5 ± 0.3 gamma per scale division compared to the maker's original value of 29.9.

The field work consisted of eight major north-south traverses and about eight minor north-south traverses, together with more random stations, and linked by a major east-west traverse. Eight base stations were established at easily accessible sites at distances of at least fifty yards from roads. The traverses were kept in as nearly straight lines as possible at right angles to the strike of the Stublick Fault line. Pacing to boundaries and sighting by prismatic compass accurately fixed base station positions. Two subsidiary stations were always set up a few yards either north-south or east-west of the bases to eliminate local near-surface

effects such as magnetic boulders in the drift. The plan of the main bases is shown in Appendix 1, together with the sequence of linking them to the main base. It was usual to return twice to base during the day on normal field work, but some days necessitated one return only. The spacing of intermediate stations depended on the detail required but usually near the fault line it was considered necessary to have fifteen yards intervals or less. The widest regular spacing was a hundred yards but two hundred yards was sufficient in some outer parts : the closest regular spacing was five yards. Nearly all stations were set up more than twenty yards from the nearest roads, fences, etc. There were a few electric fences in the area but stations were kept well away : Slight trouble was experienced with the nearness of power lines and some such readings have been rejected as being invalid. The tripod of the variometer was consistently used at minimum height to ensure maximum rigidity on soft ground and in windy weather.

The first step in the reduction of the observations was to convert them to gamma using the calibration factor. A temperature correction was not applied separately as this was automatically incorporated into the final drift correction.

In September, 1958 the writer calculated the latitude correction by comparing photographic records of the magnetic field intensity of two widely separated observatories on somewhat similar longitudes : Eskdalemuir and Stonyhurst. The differences between the two stations of the intensity were reduced for diurnal variation and the average value was taken. The resulting latitude correction was 6.8 $\pm$ 0.2 gamma per minute of latitude, increasing northwards. It is considered to be an accurate estimate and a more effective procedure than by taking values which had been calculated several years ago. It was seen previously that the regional value of the vertical component in a west-east direction changes little compared with the relatively rapid change in a north-south direction, so it was decided to use the estimate made by Bott and Masson-Smith of the longitude,

increasing westwards, of 1.0 ± 0.3 gamma per minute of longitude. These values were used in the present work. Both of the corrections were combined facilitating an easier reduction of the data, but as the total area of the survey is relatively small the greatest correction applied was only 25 gamma.

The correction for the diurnal variation, which varied little during the greater part of the field work, was made by interpolating between continuous photographic records supplied by Eskdalemuir Observatory and those lent by Stonyhurst Observatory. The variation usually corresponded to within a few gamma between the two stations. The final corrections were for closing errors. The procedure in correcting for drift was carried out in the following way :

(1). The intermediate stations were referred to the local bases every day.

(2). On the east-west base traverse the bases were referred to the first base (called the main base).

(3). On this traverse the base-pairs were adjusted to read the same by taking their averages.

(4). The main base value on the base traverse was adjusted to the value obtained on the first day and the other bases adjusted accordingly.

(5). The local base values for each day were adjusted to their now corrected values found on the base traverse and the intermediate values likewise adjusted.

Before the drift corrections were applied the base readings often disagreed considerably on the traverses even though all the corrections had been made. For instance the differences sometimes amounted to 30 or 40 gamma. It is noticeable that on days where temperatures stayed quite constant the differences were small and normal, but a separate temperature correction could not have reduced the large differences very much. This part of the reduction is therefore one of the sources of greatest error. The

other possible source of error comes in procedure (3) above with an estimate of ± 8 gamma. Both errors can be summarised under non-linearity of drift caused by (a). changes in the mechanical properties of the moving parts and (b). rapid changes of temperature. The readings at all stations are estimated to have a standard error of ± 12 gamma; this is unexpectedly rather high, but when compared with the large field anomalies the error is relatively small.

In deciding the numerical values of the anomalies the problem is always where to place the arbitrary zero, as in this type of work absolute values of the vertical intensity can not be assigned to the contours: thus the contour map is an anomaly map showing purely relative values between stations. It was thought advisable to tie in these values as closely as possible to others previously found in the area. The magnetic anomaly map of Bott and Masson-Smith (1957) was used for this purpose. It was found that the results of this survey were closely comparable with those of the above writers, and also with those of the writer's own preliminary survey. Sometimes the ties are remarkably close but the average difference is from ten to twenty gamma. (It should be noted that the values at the stations in the preliminary survey were not used in the present survey). On the isogam map (Plate 1) contours were placed at twenty gamma intervals, with a hundred gamma intervals in the regions of maximum gradients.

CHAPTER III

Description of Magnetic Anomalies

(see Plate 1)

The most impressive feature on the map is the belt of positive magnetic anomalies directed east-west in the west and east north-east / west south-west in the east. Two areas are distinguished for their high positive anomalies. They will be named after their localities, Coanwood in the west (section AB, fig. 5) and Boghead in the east (section CD, fig.6). This positive belt diminishes rapidly two miles east of Coanwood, but after a gap of about 600 yards of relatively low intensity it continues again at Boghead in an east north-east direction. It terminates almost completely just west of Coanwood, but further west the anomalies are somewhat uncertain owing to the unsuitability of the surroundings for surveying with a magnetometer (old mine-shafts and collieries, railway lines, and wooded areas). It should also be noted that in this area the Whin Sill lies very close to the surface: this may cause spurious readings.

The ridge is succeeded northwards by a broad area of negative anomalies, widest in the west, and striking in a similar direction. There is a slow rise northwards to the background field in the west, but a relatively rapid rise in the east. South of the positive ridge lies a broken zone of negative anomalies; these occur close to the ridge at Boghead but are displaced considerably southwards at Coanwood. South of this zone the background field near Boghead rises gradually to a higher value than in the Coanwood vicinity. Occasionally small positive and negative anomalies are present, perhaps within large anomalies of opposite sign, but these are relatively insignificant. It should be noted that in a small area about one mile east of Coanwood and near the Cristowell Burn, the positive ridge widens and strengthens.

Fig. 5

The COANWOOD Vertical Field Magnetic Anomaly

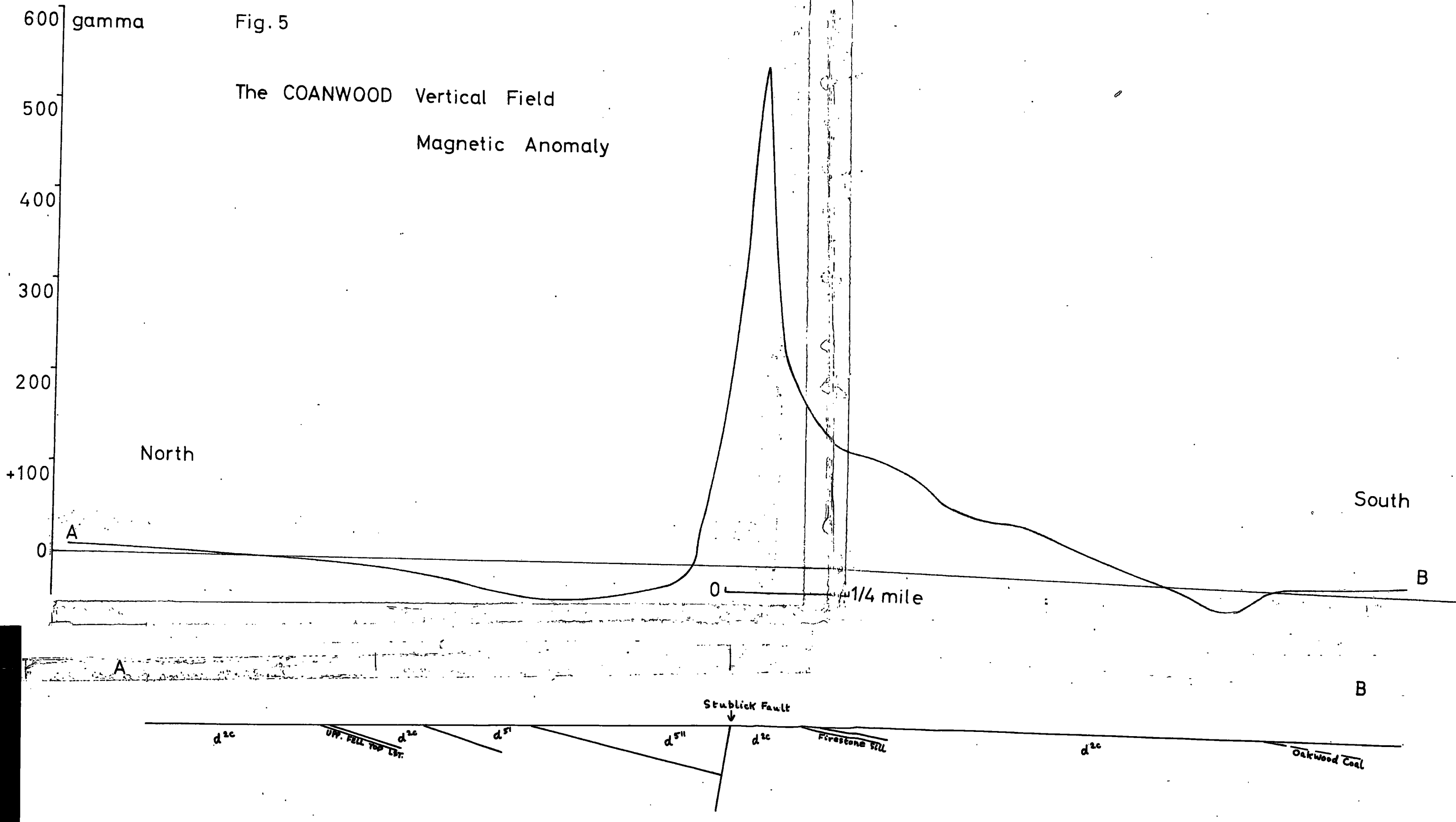

Fig. 6

The BOGHEAD Vertical Field Magnetic Anomaly

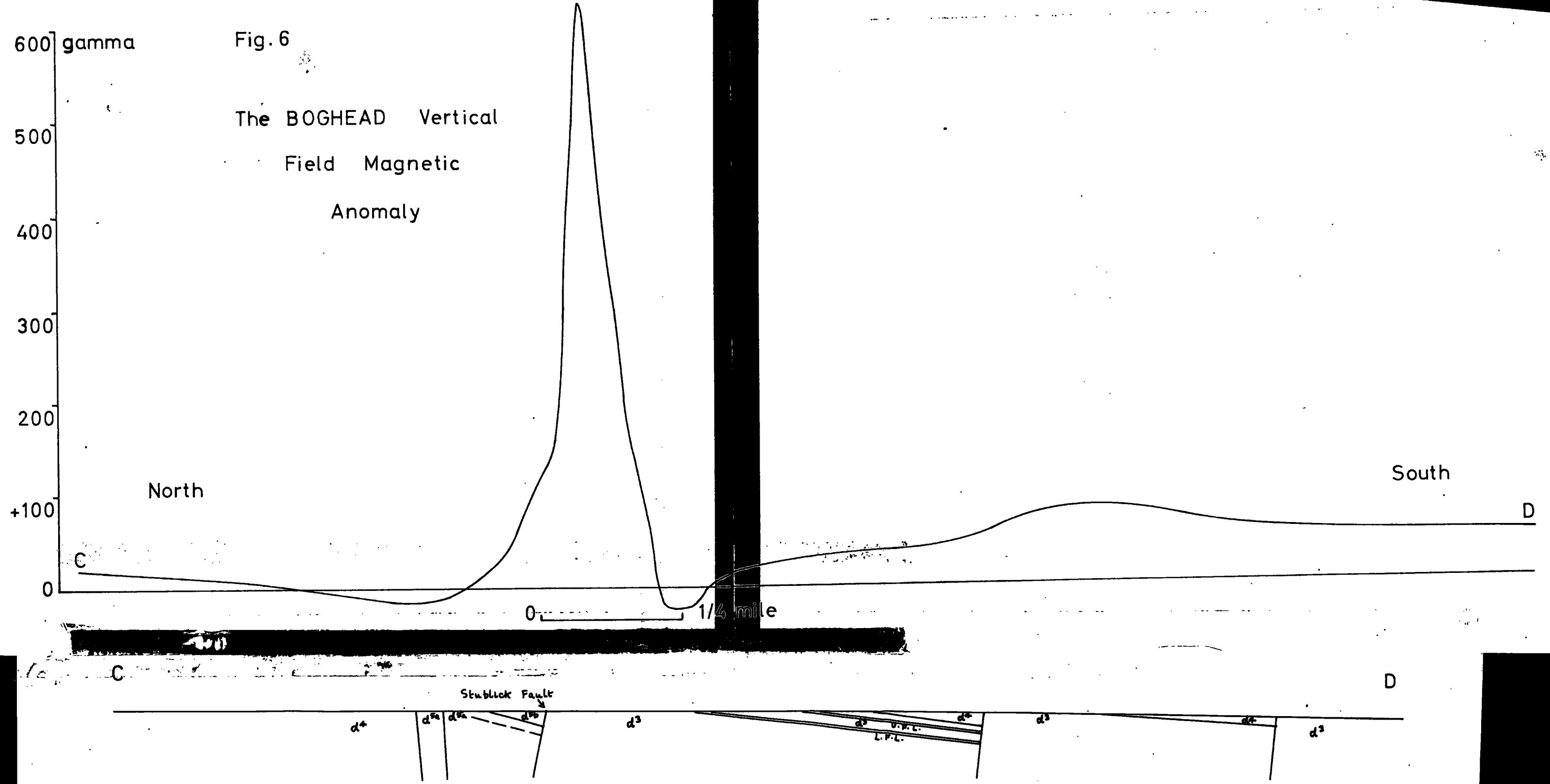

Taking the map as a whole the regional or background field is estimated at twenty to thirty gamma (see Chapter V for further discourse on this subject).

The maximum amplitude of the Boghead anomaly is about 670 gamma (fig. 6). The gradients are steep, more than two gamma per foot on the north-west flanks and about 1.25 gamma per foot on the south-east flanks. The shape is almost symmetrical and the changes of gradient are sharp. South of the positive anomaly the gradients of the negative trough are more distinct than those in the negative zone north of the positive ridge. The north-south distance occupied by the whole anomaly is 0.75 mile only. The maximum amplitude of the asymmetrical Coanwood anomaly (fig. 5) is approximately 605 gamma, and the maximum gradients on both flanks are 1.5 gamma per foot, less than the steepest Boghead gradients. However the east-west strike distance covered by anomalies of over 200 gamma is nearly 2 miles compared with only 0.5 mile for Boghead. The southern positive flank is irregular, extending a considerable distance southwards before returning to zero, to be followed by a small negative trough. The wide negative zone on the north side, more distinct than at Boghead, has spot readings of less than -50 gamma. The total north-south extent of the central positive ridge is 0.9 mile, and of the whole Coanwood anomaly, about 1.75 miles.

When contrasting the geology (fig. 2) and anomaly (Plate 1) maps the first noticeable comparison is the very close conformability of the anomaly to the geology and structure of the area. The central axis of the positive ridge corresponds to within a few feet with the line of the Stublick Fault. The termination of the ridge just west of Boghead coincides with the termination of the fault line in that area, and with a small fault running south-east into the main fault, but the actual

axis of the ridge here lies some feet north of the fault line. The ridge sharply recommences at Boghead with the beginning of the en-echelon fault line. This close relation of anomalies and structure and its significance will be fully discussed in Chapter V.

CHAPTER IV

Methods of Interpretation

(a). Introduction.

As an introduction to this chapter an attempt must first be made at explaining a magnetic anomaly. It means a natural or artificial disturbance in the earth's magnetic field, and can be great (regional) or small (local) in extent. This thesis deals only with local magnetic anomalies. Certain types of particles contained in rocks and minerals within the earth's crust become magnetic when subjected to magnetic fields such as the earth's field. This magnetisation is usually resolved into two types. These are induced and remanent (or permanent) magnetisation. The former is caused by the earth's present field, and the latter by ancient fields of the geological past. The combined effect of these two factors is to produce a magnetic anomaly by reinforcing or depleting the magnetic intensity of the earth's normal field. The former condition produces a positive anomaly, the latter a negative anomaly. Local anomalies can also be explained by artificial causes, such as underground pipes, wasteheaps, old mine workings, etc. They are usually very limited in extent.

(b). Principles of Methods.

There are two distinct methods of analysing magnetic anomalies quantitatively, each based on a different principle. The first is by pole and line theory (Heiland, 1940, pp. 380, 389*). This is independent of the strength and direction of the earth's field and only the position of the poles need be known. It is an ideal method for solving ore-body anomalies

* This should read pp. 381 – 390.

which can be very large, and where ores are relatively small structures. In the Haltwhistle problem however the structures have considerable size and the anomalies are relatively small. In such instances the anomalies are more usually directly related to the strength and direction of the earth's field, and also to the susceptibility, dimensions, and position of the body itself. The study of these relations is called induction theory and is the second method of analysing magnetic anomalies quantitatively. It has been generally applied to various two-dimensional structures such as faults, dykes, anticlines, etc. from which certain standard formulae have been evolved. The assumptions of two-dimensional analysis in this work presented no problem as the geological features are of such character as to be considered two-dimensional. However, these standard formulae have limited use. Structures often show no ressemblance to the ideal shapes stipulated in the formulae. Furthermore, the induction theory does not take into account remanent magnetism. A formula was therefore required for any two-dimensional body irrespective of its shape. It would be based on one of the standard formulae and would include the remanence factor. The theory for the development of this 'ideal' formula is described in detail in section (c).

(c). Theory and Development of Formulae.

In the induction theory certain assumptions must be made when calculating the effects of two-dimensional bodies: it is assumed that the bodies are uniformly magnetised and no consideration is given to the flux concentration on edges and corners, and also to demagnetisation effects (Heiland, 1940). Bearing these limitations in mind use is made of the very important relation between the magnetic and gravitational attractions of bodies. This is Poisson's Theorem in which

$$V = \frac{J}{G\sigma} \cdot \frac{\partial U}{\partial i} \qquad \text{- (1)}$$

where V is the magnetic potential, G is the gravitational constant, J is the intensity of magnetisation, σ is the density contrast, U is the gravity potential, and i is the direction of magnetisation.

By differentiation of (1) with respect to direction the horizontal and vertical components are

$$\Delta H = \frac{J}{G\sigma} \cdot \frac{\partial^2 U}{\partial i \partial x} \quad \text{and} \quad \Delta Z = \frac{J}{G\sigma} \cdot \frac{\partial^2 U}{\partial i \partial z} \qquad \text{- - - - - - - - - - (2)}$$

The magnetisation is then resolved into a transverse horizontal component $\underline{J}_{HV}$ and a vertical component $\underline{J}_{ZV}$, and the gravity component into a horizontal and vertical component, where $\underline{J}_{HV}$ represents the horizontal component and $\underline{J}_{ZV}$ the vertical component of the vectorial addition of the induced and remanent fields. Equations (2) then become

$$\frac{\partial V}{\partial x} = \Delta H = \frac{1}{G\sigma}\left(\frac{\partial^2 U}{\partial x^2} \cdot \underline{J}_{HV} + \frac{\partial^2 U}{\partial x \partial z} \cdot \underline{J}_{ZV} \right) \qquad \text{- - - - - - - - - - - - - - (3)}$$

$$\text{and} \quad \frac{\partial V}{\partial z} = \Delta Z = \frac{1}{G\sigma}\left(\frac{\partial^2 U}{\partial x \partial z} \cdot \underline{J}_{HV} + \frac{\partial^2 U}{\partial z^2} \cdot \underline{J}_{ZV} \right) \qquad \text{- - - - - - - - (3)}$$

$$\text{Also} \quad \Delta H = \frac{1}{G\sigma}\left(\underline{J}_{HV} \cdot U_{XX} + \underline{J}_{ZV} \cdot U_{XZ} \right) \qquad \text{- - - - - - - - - - - (4)}$$

$$\text{and} \quad \Delta Z = \frac{1}{G\sigma}\left(\underline{J}_{HV} \cdot U_{XZ} - \underline{J}_{ZV} \cdot U_{XX} \right) \qquad \text{- - - - - - - - - - - (4)}$$

where $U_{XX} = \partial^2 U / \partial x^2$ = the torsion balance curvature

and $U_{XZ} = \partial^2 U / \partial x \partial z$ = the torsion balance gradient.

If the remanent magnetism $\underline{J}_r = 0$, then

$\underline{J}_{HV} = J_{Hi} = k_i H_i \sin \alpha_i$ and $\underline{J}_{ZV} = J_{Zi} = k_i Z_i$

where k_i = susceptibility contrast in the present field

α_i = angle of strike of the body from present magnetic north

H_i = horizontal component of the earth s present field

Z_i = vertical " " " " " "

J_{Hi} = horizontal component of present field magnetisation

J_{zi} = vertical " " " " "

and $-\partial^2 U / \partial z^2 = +\partial^2 U / \partial x^2$

If remanence is involved in the calculation, then

$\underline{J}_{Hv} = \left| J_{Hi} + J_{Hr} \right|$ and $\underline{J}_{zv} = \left| J_{zi} + J_{zr} \right|$

Equations (4) can be modified further for the remanence factor. The factors $\underline{J}_{Hv}$ and $\underline{J}_{zv}$ in equations (4) can be effectively replaced by $\underline{J}_{Tv}\cos \underline{I}_{Tv} \sin \underline{\alpha}_{Tv}$ and $\underline{J}_{Tv} \sin \underline{I}_{Tv}$ respectively, where $\underline{J}_{Tv}$ = the resultant intensity of magnetisation of the total field component from the induced and remanent total fields, i. e. $\underline{J}_{Tv}$ = the apparent intensity of magnetisation (Werner, 1949). $\underline{I}_{Tv}$ = the resultant inclination of the induced and remanent total field components = the apparent inclination (Werner, 1949). $\underline{\alpha}_{Tv}$ = the resultant strike angle of the body to the resultant field component $\underline{T}_v$ = apparent strike angle. (Refer to the vector diagram in fig. 13).

Since $\underline{J}_{Tv} = \underline{J}_{iT} + \underline{J}_{rT}$ the $\underline{J}_{Tv}$ factor is easily resolved when required into the induced $\underline{J}_{iT}$ and remanent $\underline{J}_{rT}$ components. Equations (4) therefore become

$$\Delta H = \frac{\underline{J}_{Tv}}{G\sigma}\left[\cos \underline{I}_{Tv} \cdot \sin \underline{\alpha}_{Tv} U_{xx} + \sin \underline{I}_{Tv} \cdot U_{xz}\right] \text{ - - - - - - (5)}$$

$$\text{and } \Delta Z = \frac{\underline{J}_{Tv}}{G\sigma}\left[\cos \underline{I}_{Tv} \cdot \sin \underline{\alpha}_{Tv} U_{xz} - \sin \underline{I}_{Tv} \cdot U_{xx}\right] \text{ - - - - (5)}$$

- - - - - - - - - - -

Equations (5) are the basic equations from which standard formulae for various models can be developed.

An irregularly shaped body may be sufficiently approximated by

using an n-sided polygon with straight sides (Matuyama and Higasinaka, 1930 — from Heiland, 1940). By applying the gravity curvature U_{xx} and gradient U_{xz} equations for a slope, and adding and subtracting the effects of the other slopes, its gravitational effects can therefore be found. This principle has been used successfully in the interpretation of gravity anomalies (Talwani, Worzel, and Landisman, 1959). It now forms the basis for a new magnetic interpretation technique. The theory for the gravitational attraction of a slope is given below.

As only two dimensions are required, that is, the x = horizontal and z = vertical directions, the gravitational attraction of a line mass (considered very long in the y or strike direction) is calculated from its logarithmic potential U.

The potential $U = 2G\sigma \iint_S \log_e \frac{1}{r}\, dS$ (S = surface)

$= 2G\sigma \iint_S \log_e \frac{1}{r}\, dx\, dz$ (rectilinear co-ordinates) ---------- (6)

where $\iint_S$ is the surface integral,

and the gravity anomaly $\Delta g = \frac{\partial U}{\partial z} = 2G\sigma \iint_S \frac{z}{r^2}\, dx\, dz$ ----(7)

The gradient U_{xz} and curvature U_{xx} are obtained from the second partial derivative of the potential. Differentiating (7) with respect to x and z ,

$U_{xz} = 4G\sigma \iint_S \frac{xz}{r^4}\, dx\, dz$ and U_{xx} (or $-U_{\Delta}$) $= 2G\sigma \iint_S \frac{x^2 - z^2}{r^4} dx\, dz$

---------- (8)

These are the gradient and curvature expressions for a line mass; the effects of a slope are calculated by integrating (8) (from Heiland, 1940).

$U_{xz} = 2G \int_d^D z\, dz \int_{x_o}^{\infty} \frac{2x\, dx}{r^4}$ (see Appendix 2-b for diagram)

$x \equiv x_o$ on sloping edge.

Since $r_o^2 = x_o^2 + z^2$, $\psi = \alpha - \theta_o$, $r\, d\theta = dS \sin\alpha$, and

$dz = dS \sin\alpha$

Therefore $U_{xz} = 2G\sigma \int_{\theta_1}^{\theta_2} d\theta_o \sin\alpha \sin\theta_o / \sin\psi$

$$= G\sigma \left[2 \sin^2\alpha \log_e \frac{r_2}{r_1} - \sin 2\alpha (\theta_2 - \theta_1) \right]$$

But dip angle $i = \pi - \alpha$

and therefore,

$$U_{xz} = 2 G\sigma \sin i \left[\sin i \log_e \frac{r_2}{r_1} + \cos i (\theta_2 - \theta_1) \right] \quad ------ (9)$$

Similarly for the curvature,

$$U_{xx} = 2 G\sigma \sin i \left[\sin i (\theta_2 - \theta_1) - \cos i \log_e \frac{r_2}{r_1} \right] \quad ------ (9)$$

Substituting now for U_{xz} and U_{xx} in equations (5) the magnetic vertical and horizontal components for a slope are:

$$\Delta Z = \frac{J_{TV}}{G\sigma} \left\{ \cos \underline{I}_{TV} \sin \underline{\alpha}_{TV} \cdot 2 G\sigma \sin i \left[\sin i \log_e \frac{r_2}{r_1} + \cos i (\theta_2 - \theta_1) \right] \right.$$

$$\left. - \sin \underline{I}_{TV} \cdot 2 G\sigma \sin i \left[\sin i (\theta_2 - \theta_1) - \cos i \log_e \frac{r_2}{r_1} \right] \right\}$$

that is,

$$\Delta Z = 2 \sin i \, \underline{J}_{TV} \left\{ \cos \underline{I}_{TV} \sin \underline{\alpha}_{TV} \left[\sin i \log_e \frac{r_2}{r_1} + \cos i (\theta_2 - \theta_1) \right] \right.$$

$$\left. - \sin \underline{I}_{TV} \left[\sin i (\theta_2 - \theta_1) - \cos i \log_e \frac{r_2}{r_1} \right] \right\} \quad ------- (10)$$

and

$$\Delta H = 2 \sin i \, \underline{J}_{TV} \left\{ \cos \underline{I}_{TV} \sin \underline{\alpha}_{TV} \left[\sin i (\theta_2 - \theta_1) - \cos i \log_e \frac{r_2}{r_1} \right] \right.$$

$$\left. + \sin \underline{I}_{TV} \left[\sin i \log_e \frac{r_2}{r_1} + \cos i (\theta_2 - \theta_1) \right] \right\} \quad ------- (11)$$

The total field component ΔT is obtained from equations (10) and (11), $\Delta T = \Delta H \cos I_{iT} \sin\alpha_{iT} + \Delta Z \sin I_{iT}$ ---------- (12) (Ewing and Press, 1952), where I_{iT} = angle of dip of the present total field component, and α_{iT} = strike angle of the body from present magnetic north.

(d). Application of Electronic Computer.

The magnetic formulae for a slope in equations (10) - (12) are complete for both induced and remanent magnetism. They are in such a form as to be used directly for calculating profiles over irregularly shaped bodies in the way suggested by Matuyama and Higasinaka (1930) and referred to previously in this chapter (see fig. 7). The formulae are extremely tedious and time-wasting to work out manually for even a simple shape. A programme was therefore devised in 'Autocode' for use (in this form) with the Ferranti Pegasus electronic digital computer of King's College Computing Laboratory at Newcastle-upon-Tyne. A complete flow diagram of this programme, together with explanations of the trigonometry involved and a specimen of the programme in code, is to be found in Appendix 2(a) - (c).

At the Computing Laboratory the working procedure is as follows: a data tape is punched on equipment provided, on which are details of the body co-ordinates and magnetic field: a 'station' tape is punched on which are the desired number of field points. On the computer itself, after the insertion of the preliminary machine tape, the programme is fed in, followed by the data tape, and lastly the 'station' tape; immediately the first station is read in the computer begins to calculate. A typical data tape of one slope or edge would be punched in the following sequence, excluding the various coded orders: strike angle to the present field, present dip angle, slope co-ordinates, apparent intensity of magnetisation, apparent strike angle, and apparent inclination. That is, $\alpha_{i'}$, $I_{i'}$, $x_1 z_1$, $x_2 z_2$, $\underline{J}_{TV}$, $\underline{\alpha}_{TV}$, and $\underline{I}_{TV}$. A typical example of input data is shown in Appendix 2 (d-i).

From the above account it should be realised that a thorough vector analysis† of all existing magnetic and palaeomagnetic data must be accurately correlated and completed

† i.e. the simple graphical determination of the above factors $\underline{J}_{TV}$, $\underline{\alpha}_{TV}$, and $\underline{I}_{TV}$: e.g. see fig. 13, and page 30.

Fig.7 Induction Theory applied to a 2-D Polygon

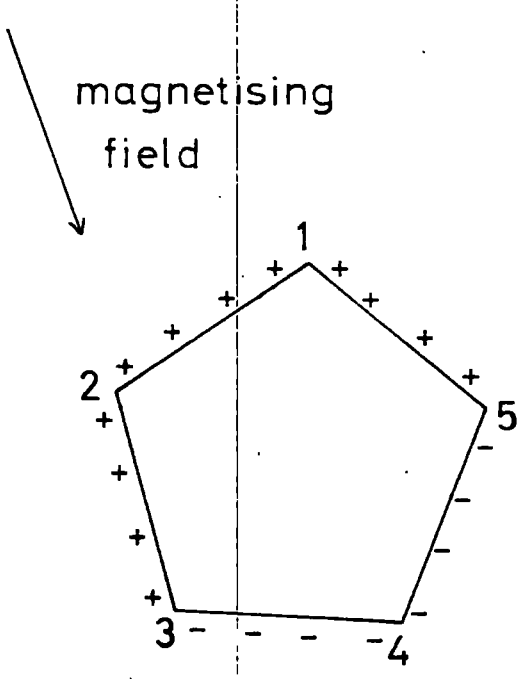

anomaly = (1+2+5)-(3+4)

before insertion into the computer. Another point, previously mentioned, is the placing of the origin. In this programme it is on the south side of the body with an anticlockwise procedure around the body edges (fig. 7). Failure to comply with these rules will produce wrong results.

The computed results are printed on paper, a specimen of which is reproduced in Appendix 2 (d-ii). The horizontal co-ordinates of the stations at whose points the effects of a body are to be calculated, are listed first as x_{ST} and y_{ST}. The three remaining columns represent the computed values of the vertical field component Z, the horizontal component H, and the total field component T (printed as F in the specimen output contained in Appendix 2). The various size and depth co-ordinates of the body to be calculated, together with magnetic data, are usually printed at the head of the results columns. Out of the Z, H, and T columns, in the interpretation of the Haltwhistle anomalies use was only made of the vertical field results Z because the magnetometer used in the field measured only the vertical component of the earth's field. The programme has however been designed also for use in the interpretation of horizontal and total field anomalies. A description of how the computer method is actually used in the quantitative magnetic interpretation is given in section (e).

(e). Interpretation Procedures.

When presented with a new magnetic anomaly certain assumptions must be made about the shape of the body causing it, e.g. a fault, dyke, sill, etc. The interpreter's knowledge of the structure of the investigated area would limit the number of possible assumptions about the shape of the body. The next task is to make out data and station tapes to be used with the new programme on the computer. On these tapes

must be included all combinations of body and magnetic parameters. In the case of a dyke for instance there are many variables to be considered, the shape and depth factors, the susceptibilities, and the magnitude and direction of the possible remanent magnetism. Thus theoretical profiles are rapidly calculated for all these varying conditions for a series of points over the body.

The sets of values are then 'normalised' by scaling the maximum amplitude of the anomalies, and occasionally their horizontal dimensions, to some convenient standard. In order for a theoretical anomaly to fit the observed anomaly within reasonable limits many attempts at varying the depth and magnetic parameters are usually necessary. If a suitable fit is found, that particular model is then considered to be a satisfactory solution to the physical interpretation of the observed anomaly. Failure to obtain a solution in this way results in a complete revision of the assumptions of the shape of the body. The whole procedure as described above must therefore be repeated again. A detailed description of these interpretation procedures for the solution of magnetic profiles, including new criteria developed specially for this work, will follow in the next chapter.

In conclusion it may be said that this computer method of solving magnetic anomalies is both faster and more accurate, more variable parameters are considered, and the period of machine operation / cost ratio is relatively low compared to the laborious and often inaccurate conventional interpretation methods. Thus for as many field points as are considered necessary for plotting accurate magnetic profiles, and for every conceivably shaped two-dimensional body situated anywhere in the world, can be calculated rapidly and accurately vertical, horizontal, and total field profiles across the centre of the body and at right angles to it, using both present and remanent magnetic data. The method is considered to be one of the most useful tools devised for the interpretation of local and regional magnetic anomalies.

CHAPTER V

Interpretation

(a). Introduction.

Considering the Haltwhistle anomalies it is evident from the 'half-widths' (see figs. 5 and 6) that their causes occur at relatively shallow depths. The basement in this region lies at a great depth (see p. 2). Thus, any hypotheses involving the basement in order to explain these anomalies are clearly inadmissable.

However, variations of the polarisation contrast (or intensity of magnetisation $\underline{J}$) can suitably explain the anomalies. Such polarisation contrasts are caused by either changes of $\underline{J}$ in the same rocks, or by changes of rock type, each possessing different $\underline{J}$ factors. The latter condition is, however, more usual.

(b). Example of interpretation procedure - the Hett Dyke.

An idea of the shapes of the disturbing bodies near Haltwhistle had been formulated during the preliminary investigations in 1958. Then the theoretical profiles were calculated manually using conventional interpretation methods. The assumed shape was that of a two-dimensional dyke, its lower end regarded as at infinite depth. This model was therefore adhered to at the beginning of the present interpretation, and because other geological structures were less likely to produce better solutions. Comparison of the Haltwhistle anomalies with others over known structures justified this initial conclusion. One particular case which has been deliberately applied for comparative purposes is the well known Hett Dyke of Co. Durham.

This dyke has been well described by many workers (Holmes and Harwood, 1928 : Teall, 1884). Of similar age and belonging to the Whin Sill Group it strikes at an angle of

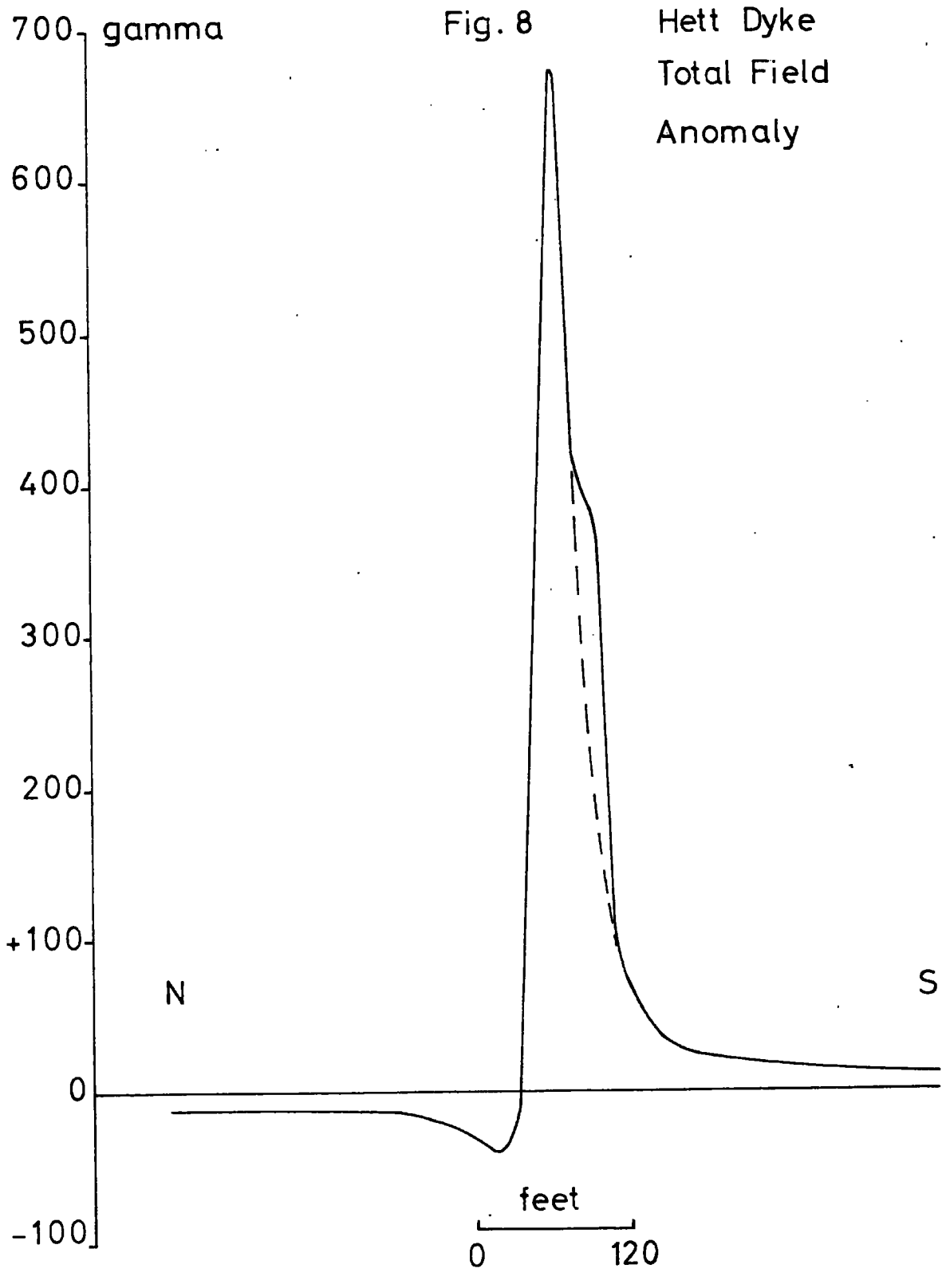

Fig. 8 Hett Dyke Total Field Anomaly

70° to present magnetic north. A survey was performed early in 1960 near Willington using a new total field proton precession magnetometer belonging to the Durham Colleges Department of Geology. A total field profile over the Hett Dyke is shown in fig. 8. In this particular area the dyke dimensions were quite well known, and the depth was estimated from the geology and topography. Holmes and Harwood (1928) observed an average width of 12 feet and the depth to the top was estimated at 12 feet also. The depth to the lower end was considered to be 1500 feet originally but this was later increased to about 13 miles, near the Curie Point geotherm. Both the intensity $\underline{J}_{TV}$ and the apparent inclination $\underline{I}_{TV}$ were unknown.

Magnetic profiles were computed for these and other dimensions, together with other varying factors, for the purpose of determining how these variations affected the size and symmetry of the profiles. Total field profiles in fig. 9 are for varying inclinations $\underline{I}_{TV}$ of the apparent field direction of magnetisation for which the ratios of positive to negative gamma vary considerably. The curve for the vertical field in fig. 10 summarises this point. Fig. 9 also shows how the axes of the positive peaks diverge from, and those of the negative peaks converge to, the central axis with decrease of inclination from 90°.

The ratio of the positive to negative anomaly is however of the greatest importance, for it is this factor which is primarily determined by the direction of polarisation. It is fundamental that this ratio should be known with some accuracy. Unfortunately it also depends directly upon another factor, often difficult to determine. This is the value of the background field. It is obvious that any slight change in the baseline will produce a relatively large change in the positive / negative ratio and so it is essential that the background field should be known accurately.

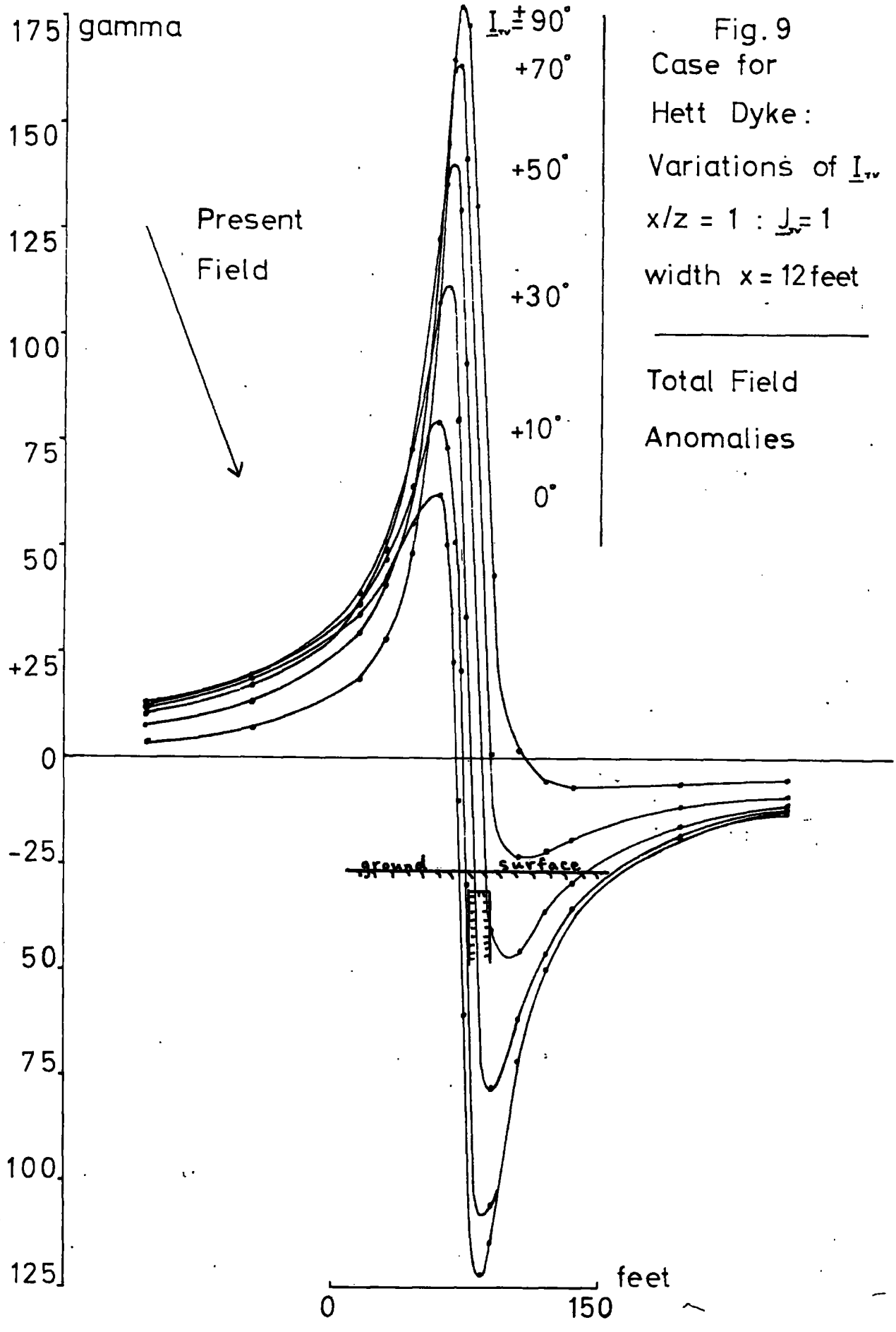

Fig. 9
Case for
Hett Dyke:
Variations of $I_{\tau v}$
$x/z = 1 : J_{\tau v} = 1$
width $x = 12$ feet

Total Field
Anomalies

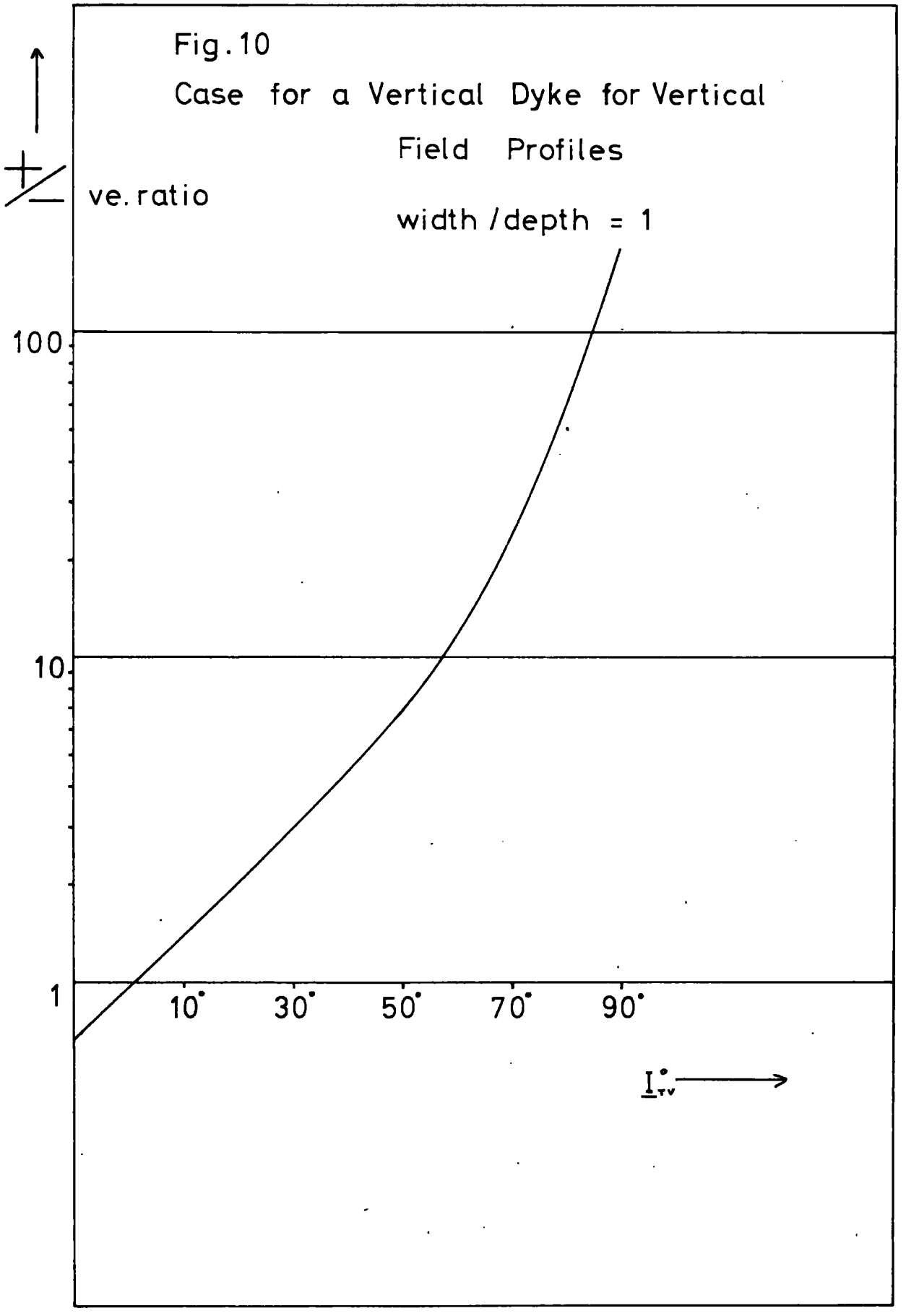
Fig.10
Case for a Vertical Dyke for Vertical
Field Profiles
width /depth = 1
+/−
ve. ratio
100
10
1
10°
30°
50°
70°
90°
I°tv

It is found convenient to use ratios when dealing with size and depth. In figure 11 are shown curves for varying width / depth ratios, the depth remaining constant. Although the amplitude varies non-linearly the profile width is directly proportional to the body width for constant width / depth ratios. Following an increase in the width / depth appears a divergence of the maximum and minimum peaks and a steepening of gradients. Considering only the amplitudes of the maxima and minima, figure 12 shows a linear decrease of the positive / negative factor with an increase of the width / depth ratio. There is little variation in the positive / negative ratios for width / depths smaller than 2.0 : it would be possible to determine the apparent inclination $\underline{J}_{TV}$ to within about 5° except when these ratios exceed 2.0.

Changes in the strike angle (Jakosky, 1950, p. 217) cause a shift of the maximum and minimum peaks relative to the cetral axis of the body, and a change in their amplitudes. Another effect concerns the positive / negative ratio. Unexpectedly it was found that as the strike angle decreased (in this instance to the apparent direction of magnetisation) the positive / negative ratio decreased considerably by enlarging the negative value. However, variations of this angle from 80° to 90° cause an almost negligible change in the positive / negative ratio. Fortunately the values for the Hett Dyke were thought to lie near or within this small range. A variation of the intensity of magnetisation $\underline{J}_{TV}$, although often difficult to resolve from the width and depth factors, produces no new changes, the gradients, width, and amplitudes being directly proportional to $\underline{J}_{TV}$: the positive / negative ratio is unchanged assuming other factors remain constant.

Fig.11 Total Field Theoretical Profiles for a Vertical Dyke

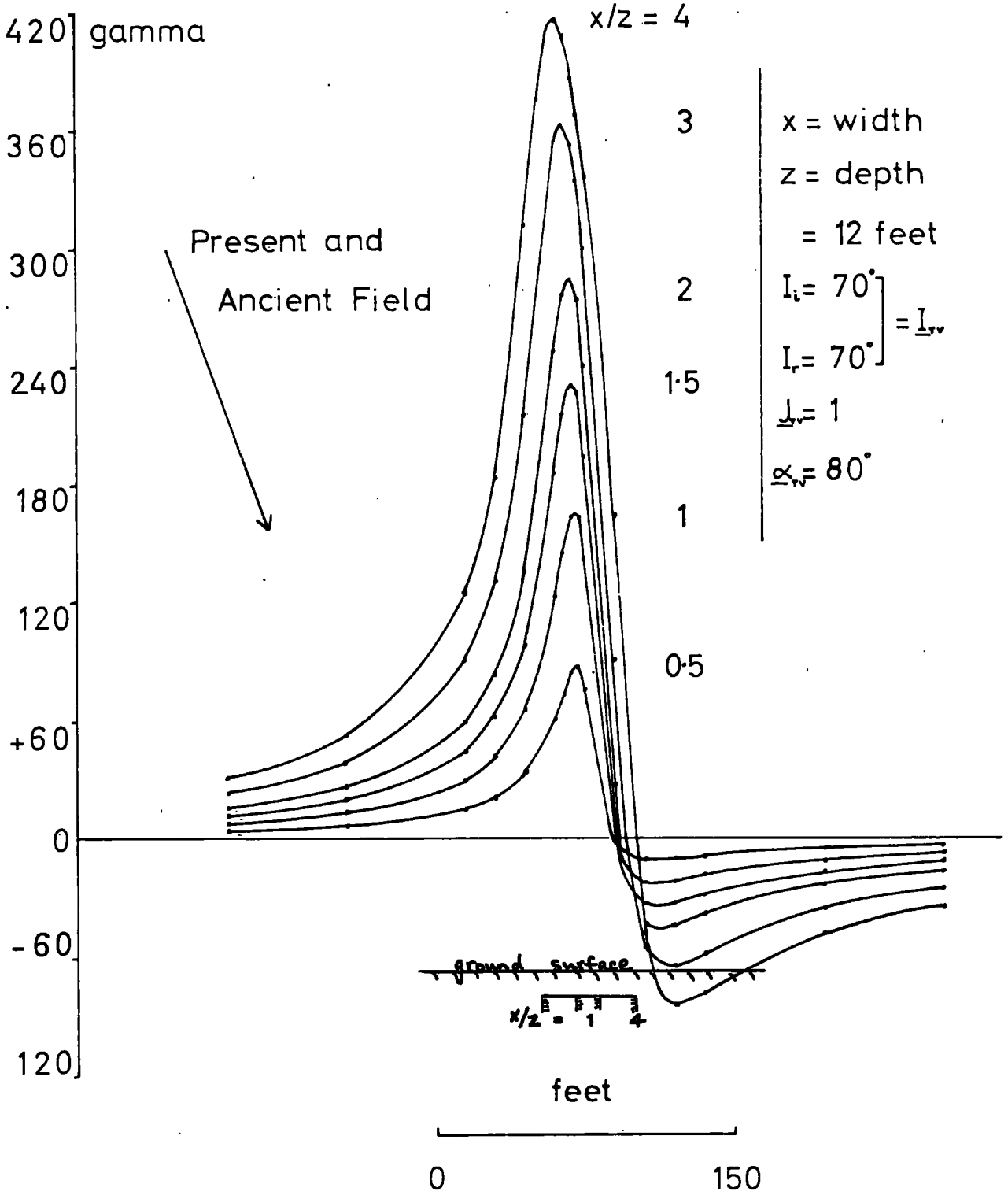

From the above account it appears that the most fundamental item to be solved in a field profile is the apparent inclination $\underline{I}_{TV}$. The use of positive / negative ratios seems to provide the most effective answer. Having obtained this inclination it should be possible to determine the apparent intensity of magnetisation, either from a graphical construction using the present field intensity as unity, or later from the size and depth factors. The determination of the size and depth is made more simple if a slight idea is known of one or the other factor. This is an oversimplified picture of the most effective method used up to date, involving both quantitative and graphical techniques.

Following the preliminary introduction of this method (first mentioned in the last chapter) the procedure for solving field profiles is as follows :

(1). The positive / negative ratio of the field profile is measured.

(2). Profiles are computed for various apparent inclinations $\underline{I}_{TV}$ and different width / depth ratios using $\underline{J}_{TV}$ as unity : the positive / negative ratio of each profile is found and plotted on logarithmic graph paper against the corresponding inclinations for the different width / depths as shown in one example in fig. 10.

(3). The value of the observed ratio is located in this figure and a horizontal line drawn from this point on the ordinate to intersect some of the curves. Along this line there are several possibilities of the apparent inclination $\underline{I}_{TV}$ for varying width / depths.

(4). Using these values of the inclinations and letting $\underline{J}_{TV} = 1$, various profiles are computed for these different width / depth ratios.

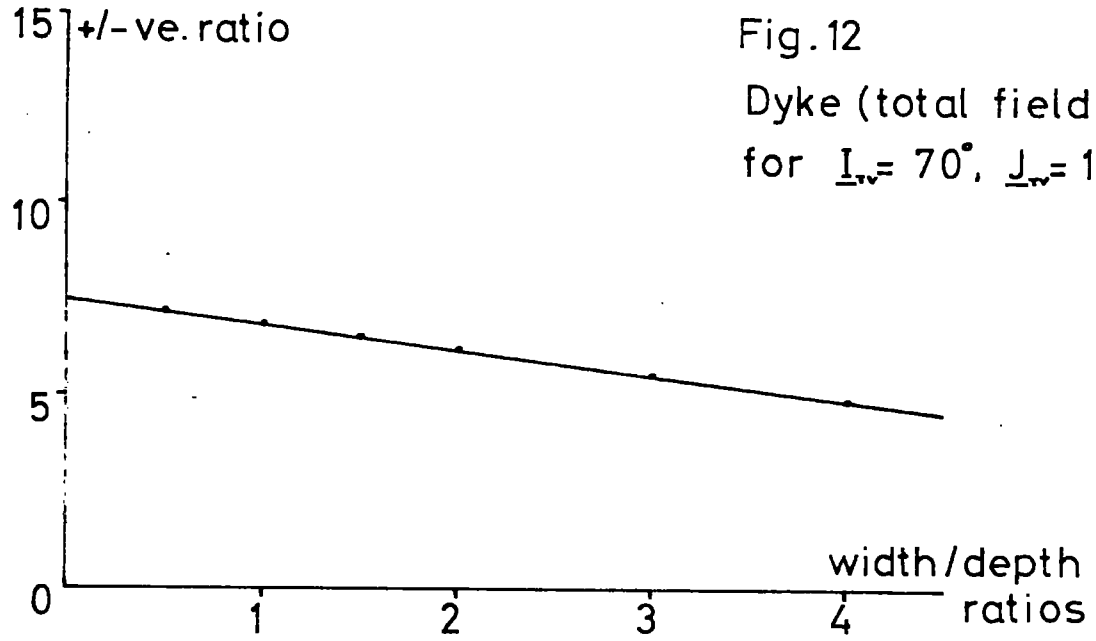

Fig. 12
Dyke (total field)
for $\underline{I}_v = 70°$, $\underline{J}_v = 1$

Fig.13 3-D Vector Diagram of the Whin Sill Magnetism.

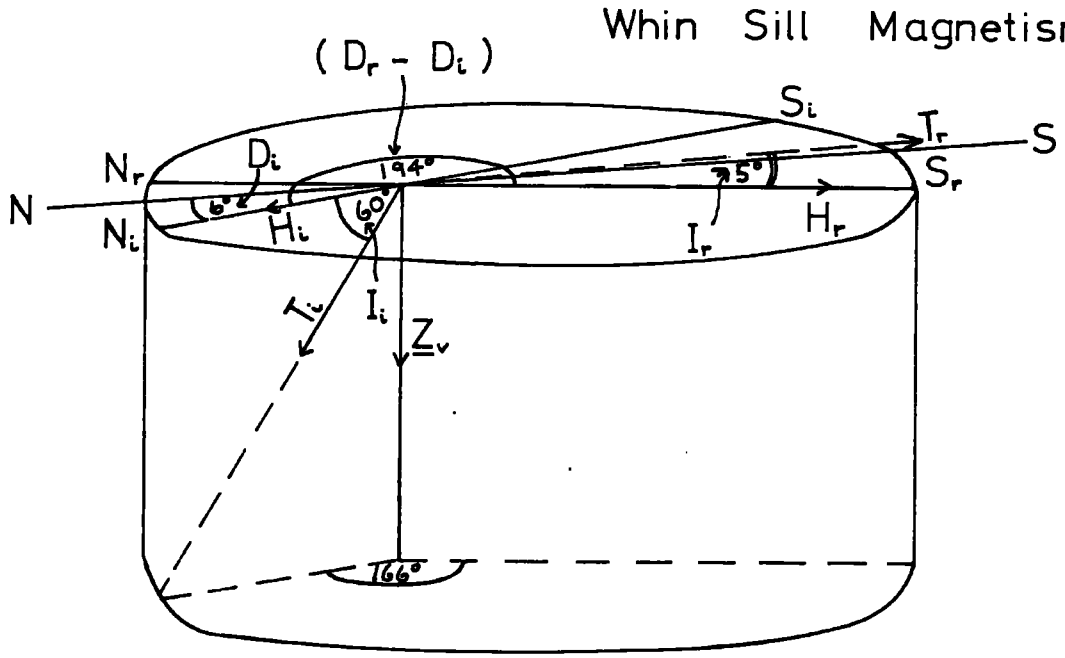

(5). The observed and calculated profiles are scaled to the same amplitudes and half-widths, but if either the depth or the width have been assumed only the amplitude needs scaling. The closest fit between the observed and calculated profiles is taken as the most satisfactory solution for the observed profile. The correct theoretical profile is then scaled to its original value, the factor by which this is done being a measure of the width or depth, and the apparent intensity of magnetisation $\underline{J}_{TV}$.

The Hett Dyke example under consideration has proved to be simple because the width was known with reasonable accuracy. In many cases however the width is more unknown than the depth, but it is no difficult task to assess these two factors using this method. The apparent inclination $\underline{I}_{TV}$ is about 80° for the Hett Dyke. The strike of the body to the ancient field was unknown but it was assumed to have a similar angle to that of the present field. The known width of 12 feet was taken as unity. The closest fit was between the curves for width / depths 2 and 1 , and thus the depth to the dyke was assumed to be between 6 and 12 feet, a value in close agreement with the geology and topography of the area. Although by no means a difficult problem, the Hett Dyke example - - - - - - - - -

has provided valuable techniques for the purpose of solving the considerably more difficult case of the Haltwhistle anomalies.

(c). Physical Interpretation of the Haltwhistle Magnetic Anomalies.

A close look at the Coanwood and Boghead profiles (figs. 5 and 6) reveal one obvious feature in common with the Hett Dyke profile: the positive peaks lie distinctly south of the negative peaks suggesting a completely normal polarisation direction. The observed positive / negative ratios corresponded to an inclination of about 70° (fig. 10) for a vertical dyke assuming a background field of 25 gamma and width / depth of unity. The close similarity of the profiles to that of the Hett Dyke encouraged a possible solution by supposing the anomalous body to have a dyke form.

However the first step in the present interpretation of the Coanwood and Boghead anomalies was to discover the geophysical effects of the Stublick Fault on the Whin Sill. It had been supposed that these effects would be only relatively slight. The following paragraph deals with some of the magnetic aspects of the Whin Sill.

The preliminary interpretation of 1958 was based entirely upon the assumption of normal magnetisation only. However, work by Creer and others (1959) and Hallimond and Butler (1949) has shown that for the Whin Sill there is a considerable component of remanent magnetism which is directed almost horizontally southwards. This was an interesting revelation which would in all probability result in a differently shaped calculated profile for a faulted slab. The Whin Sill figures were taken and the results averaged. The data used in the first calculations are as follows (from Creer and others, 1959):

remanent declination $\underline{D}_{rT} = 188°$

remanent inclination $\underline{I}_{rT} = -5°$ (or 185°)

normal remanent magnetism (NRM) = $\underline{J}_{rT}$ = 27.9×10^{-4} cgs. units
susceptibility k_{iT} = 19.8×10^{-4} cgs. units
and NRM / k_{iT} = 1.4 .
This susceptibility value was used in finding the induced magnetism, assuming the present total field had a value of 0.5 oersted; i.e. $\underline{J}_{iT} = k_{iT} T_i$ or $\underline{J}_{iT} = 19.8 \times 10^{-4} \times 1/2 \approx 10^{-3}$ cgs. units. Therefore the Koenigsberger ratio $\frac{\underline{J}_{rT}}{J_{iT}}$ = 2.8 .

The next step was to find the apparent inclination $\underline{I}_{TV}$ and the apparent intensity of magnetisation $\underline{J}_{TV}$. In this instance the present dip $\underline{I}_{iT}$ was used at 60° and the declination $\underline{D}_{iT}$ at -6° (see fig. 13). It was calculated that the apparent inclination $\underline{I}_{TV}$ = +165° and the apparent intensity $\underline{J}_{TV}$ = 2.4×10^{-3} cgs. ; the apparent strike angle $\underline{\alpha}_{TV}$ was taken at about 90° but more correctly it should have been about 100°. However, as will be seen later, a difference of 10° of strike angle near 90° produces little change in a profile shape. From the one inch Geological Survey map (Brampton Sheet) the Whin Sill dips gently south south-eastwards south of the Stublick Fault, at an angle of 10°. It is not known whether the rock solidified at this angle or whether it first solidified in a horizontal plane and was tilted later. Assuming the latter in this example the apparent inclination $\underline{I}_{TV}$ was therefore taken to be about +155°. From the single exposure of Whin Sill in the area (Lambley quarries, near Coanwood) and from the Brampton Sheet and one inch Ordnance Survey map the thickness was estimated at approximately 100 feet. Along the Coanwood profile at the point of maximum positive value the depth was estimated at about 150 feet, assuming a tilt of 10° of the sill. Both these estimates were regarded as being quite accurate. From the geological map the actual depth to the sill on the down-thrown side is about 3000 feet in this region. In assuming an

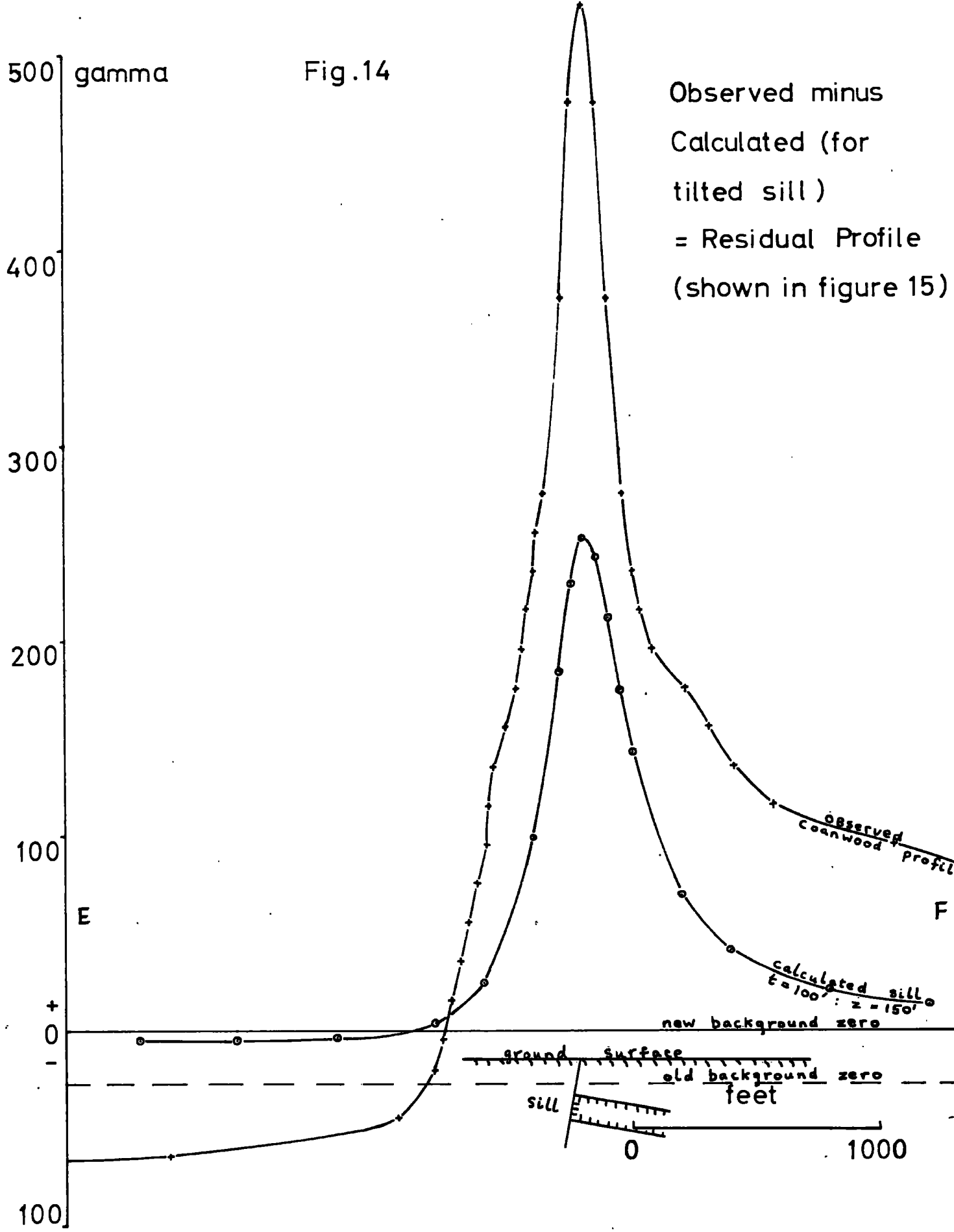
500
gamma
Fig.14
Observed minus
Calculated (for
tilted sill)
= Residual Profile
(shown in figure 15)
400
300
200
100
E
F
Observed
Coanwood
Profil
Calculated sill
t = 100'
z = 150'
+
0
-
new background zero
ground surface
old background zero
feet
sill
0
1000
100

infinitely thrown side half the time available on the computer is saved, and again, the time used in calculating for a tilted sill is three times longer than for a horizontal sill.*

The computed profile is shown in fig. 14. The background zero of the Coanwood profile (fig. 5) has been adjusted to a new level on the basis of investigations to be described later. Considering the Coanwood profile only, the computed profile (fig. 14) was subtracted from it producing the residual curve given in fig. 15. Assuming all the effects of the faulted sill had been cancelled out the inference was that this residual profile was wholly caused by some other body. However, it was realised that the 1958 interpretation of a dyke was no longer suitable and the data supplied by the Hett Dyke would not apply to this problem owing to the large reduction of the positive / negative ratio of the residual curve. Doubt was also cast on the genuity of the shape of this curve, although its irregularities were smoothed out as far as possible. The observed ratio of 4.4 corresponded to an apparent inclination $\underline{I}_{TV}$ of 40° (fig. 10). There were no hopes of obtaining an easy solution using the Hett Dyke normal inclination of 70° - 80°. In the residual curve (fig. 15) the top segment AB was regarded as variable owing to its doubtful existence. This was acceptable because all of this portion could be eliminated merely by increasing the intensity slightly or by decreasing the depth. A value of 225 gamma for the positive side was adhered to in the computation, resulting in a positive / negative ratio of 3.6 and inclination $\underline{I}_{TV}$ of 35°. The width of the hypothetical dyke was assumed to be 300 feet and the depth to the top was varied: z/x values of 1/4, 1/2, 1, 2, and 4 were used. The upper northern edge of the dyke was placed theoretically directly below the Whin Sill and in contact with the plane of the fault. The apparent inclination $\underline{I}_{TV}$ of 35°, together

* The extent of the error in ignoring the downthrown side is, in the case of the positive/negative ratio, less than 2%.

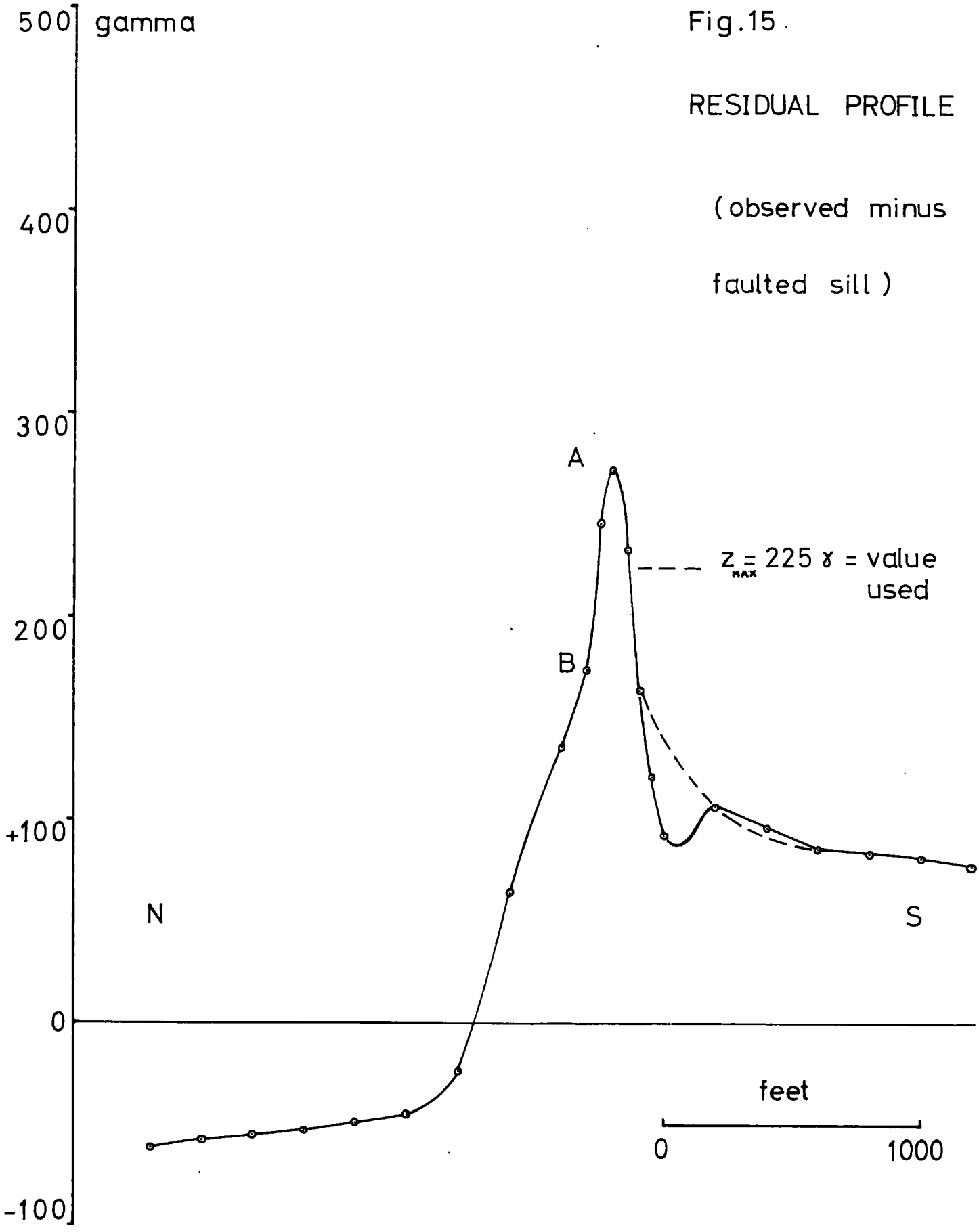

Fig.15

RESIDUAL PROFILE

(observed minus faulted sill)

with the above dimensions for a vertical dyke, were used in the calculation, the reduced profiles (reduced to $z/x = 1$) appearing in fig. 16. It became obvious that the lateral parts of the calculated curves were not similar to those of the residual curve. The negative side of it had an area too large to be explained by the inclination used. Decreasing the inclination or increasing the width would only produce a profile wider than the observed. Fortunately a very important point emerged which later proved to be a vital factor in the interpretation. Using an inclination of +35° for the dyke had an adverse effect on the profile. The field position of the positive peak diverged considerably from the central axis: for $z/x = 1$ this southward shift amounted to 100 feet for $x = 100$ feet and 300 feet for $x = 300$ feet. This divergence of axes had previously been observed during work on the Hett Dyke. As a result, two possibilities were inferred. Either that the dyke's central axis should be placed somewhat north of the fault, in which case it would be more acceptable geologically if the axis was inclined so as not to cut the fault plane. Or that it would be wiser policy to search round for another possibly more simple mechanism to account for the close coincidence of the observed maximum with the fault plane position. It appeared therefore that the residual profile could not after all be easily explained by using a model dyke. It seemed likely that some other source was exerting its influence upon the lateral parts of the observed profile, perhaps of deep seated origin.

It was ultimately realised that an important factor had indeed been neglected. This was the effects of faulting the basement rocks. Unfortunately any calculations concerning these rocks must necessarily be speculative owing to the lack of palaeomagnetic data. From previous work however in Northern England (Bott and Masson-Smith, 1957) it seems likely that the

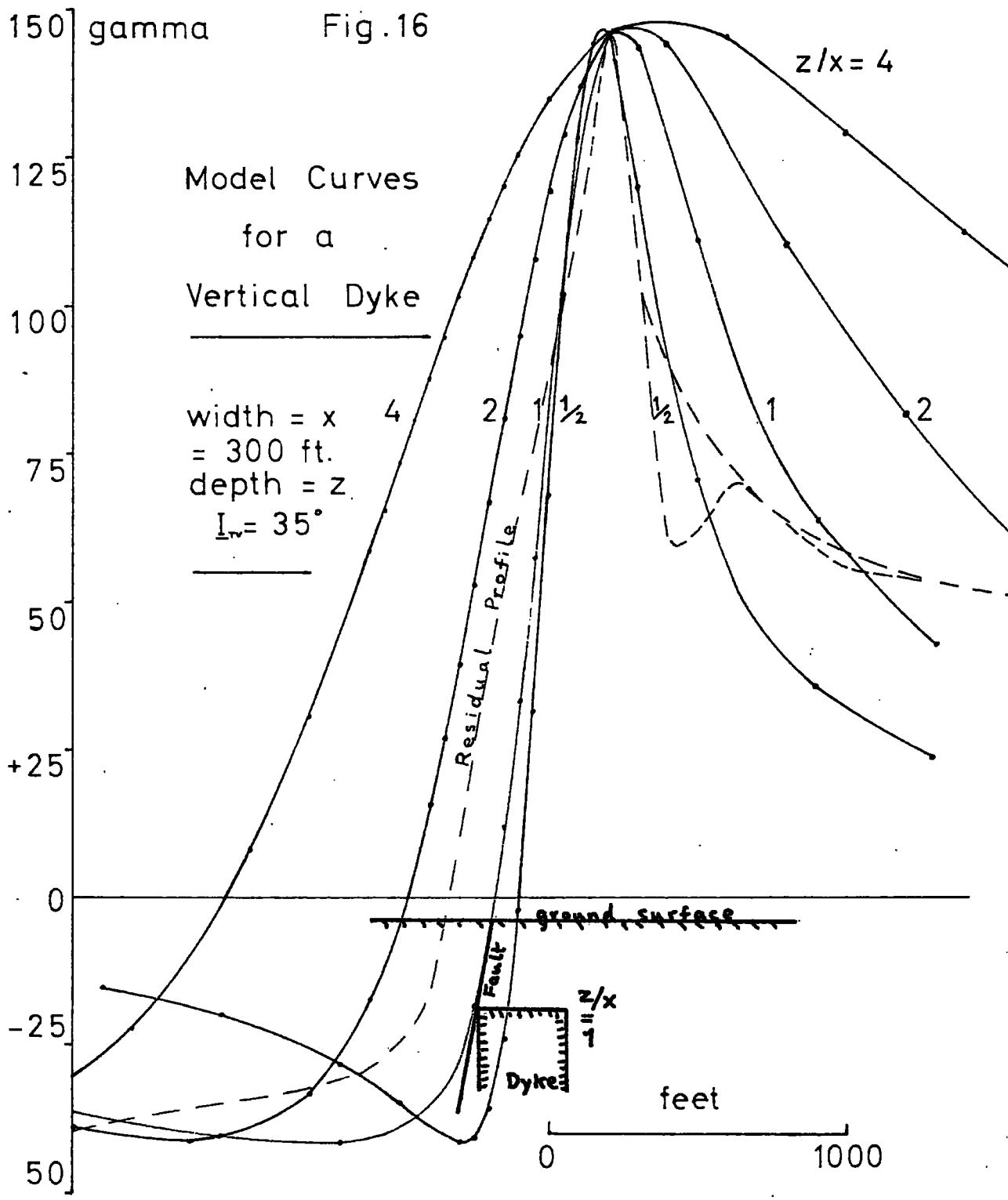
150
gamma
Fig. 16
125
100
75
50
+25
0
-25
50
Model Curves
for a
Vertical Dyke
width = x
= 300 ft.
depth = z
I_m = 35°
4
2
1
1/2
1/2
1
2
z/x = 4
Residual Profile
ground surface
Fault
z/x = 1
Dyke
feet
0
1000

direction and inclination of the remanent field for these rocks are similar to those of the induced field: the figures used were $\underline{I}_{TV} = 70^{\circ}$ and $\underline{\alpha}_{TV} = 97^{\circ}$. Another unknown was the depth to the basement rocks on the south side of the Stublick Fault, but it was considered unlikely that it would exceed 1500 to 2000 feet (Dunham, 1948: Trotter and Hollingworth, 1932). Two profiles were obtained for depths of 1500 and 2000 feet shown in fig. 17. The negative part of the curve for the former value is considered to be too great compared to the observed, and so for all further work the latter value was accepted.

From what had been said in the previous paragraphs, although the possibilities of a dyke could not altogether be excluded, the residual profile could be discarded temporarily. Proceeding on a different line of approach a new residual profile (fig. 18) was constructed by subtracting the basement profile from the observed. It was noticeable that there was some similarity between this curve and that for the tilted sill of figure 14. Perhaps the new residual profile might be entirely explained by varying some of the magnetic data and dimensions of the Whin Sill. This suggestion prompted immediate action in which a thorough model analysis was performed and described in the following paragraphs.

In the earlier stages of the interpretation the average values of the palaeomagnetic measurements (Creer and others, 1959) were used. These could be varied however, to the limits of the individual values from which the averages were taken. The extreme ranges are as follows:

	Referred to present horizontal	Corrected to bedding
Declination :-	169° to 205°	171° to 205°
Inclination :-	-25° to +28°	-28° to +18°

Similarly the NRM from five exposures varied from 19.9 to 40.0 x 10^{-4} cgs. (average = 27.9 x 10^{-4} cgs.).

Fig .17

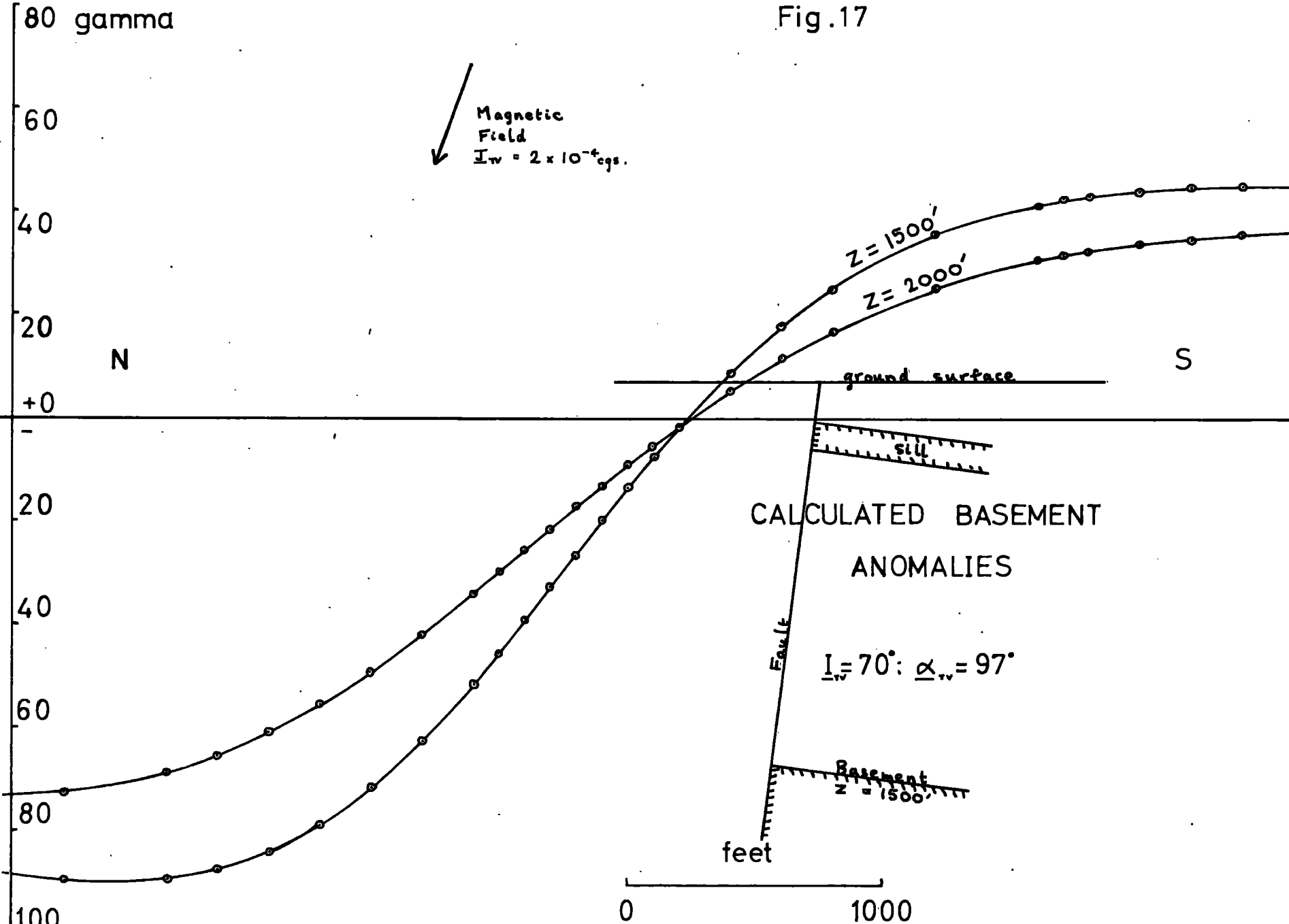
80 gamma
60
40
20
+0
20
40
60
80
100
N
S
Magnetic
Field
I_w = 2 x 10⁻⁴ cgs.
Z = 1500'
Z = 2000'
ground surface
sill
CALCULATED BASEMENT
ANOMALIES
Fault
I_w = 70°: α_w = 97°
Basement
Z = 1500'
feet
0
1000

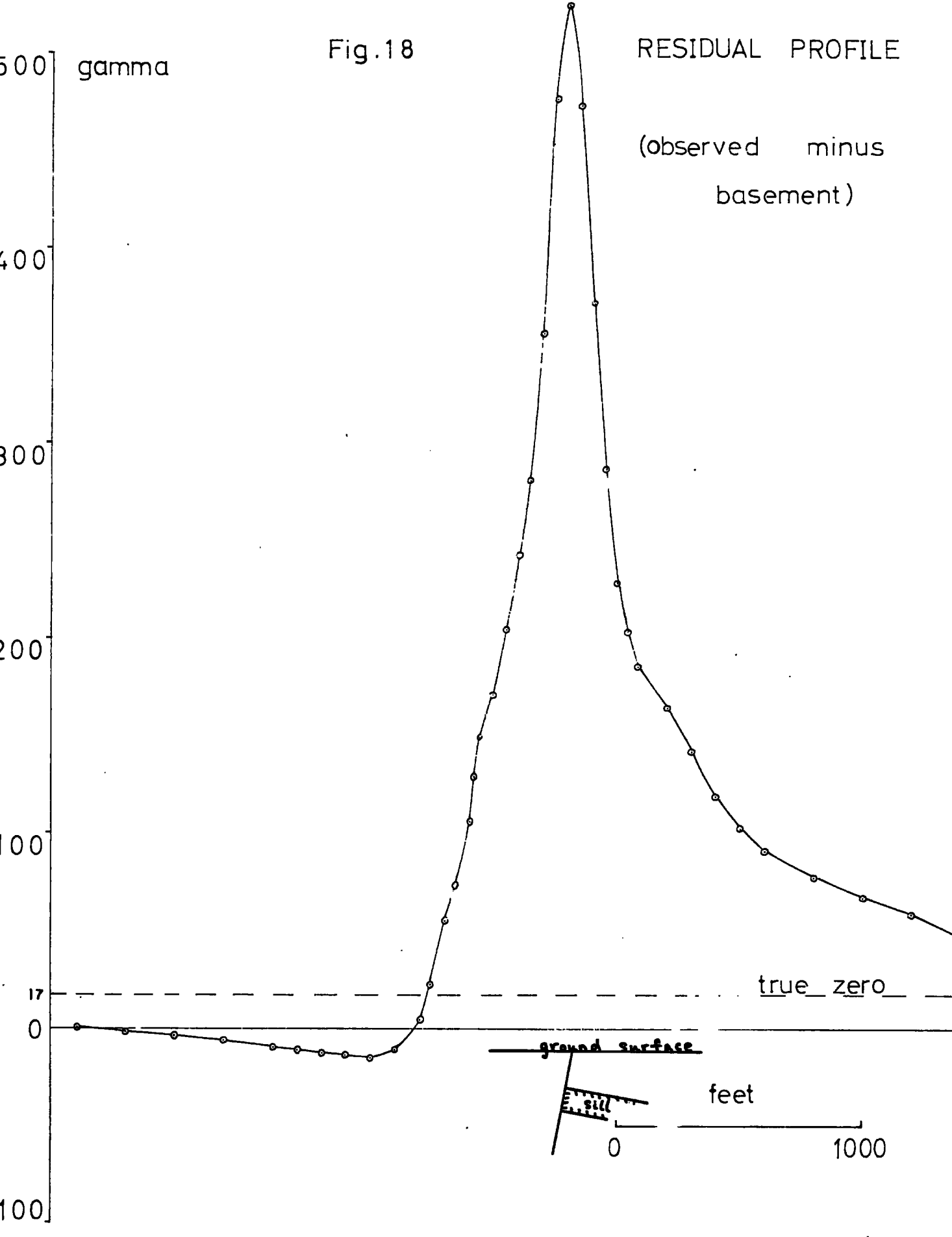
Fig.18
RESIDUAL PROFILE
(observed minus basement)
gamma
500
400
300
200
100
17
0
100
true zero
ground surface
sill
feet
0
1000

Knowing that a fair degree of latitude could be allowed for in the Whin Sill interpretation the next task was to ascertain the values of the background field. The basement anomalies complicate this evaluation considerably. The method by which it was carried out is as follows. Values of the basement anomaly were computed to distances of over one mile north of the positive anomaly ridge (see anomaly map, Plate 1). At such distances it was considered that the effect of the faulted sill would be negligible. Assuming no other external factors influence the area the observed anomalies are entirely due to basement faulting. The calculated anomaly 6000 feet north of the fault is -17 gamma compared to the observed value of +10 gamma. This means that all the observed magnetic readings on the anomaly map are in reality 27 gamma too high. In section AB, fig. 5, the true positive value should be 523 gamma and the negative value, -69 gamma, as shown later in fig. 14. But the true background value is the basement zero. Therefore the observed base line should be adjusted to the new value of +17 gamma. This corresponds to a background of +27 gamma on the anomaly map, a value in close agreement with an earlier estimate. A new residual profile was constructed (referred to previously in fig. 18) on subtracting the basement profile from the corrected observed profile.

Using the Whin Sill data given earlier in this chapter, for different thicknesses and inclinations $\underline{I}_{TV}$, for constant depth, curves were computed for a horizontal faulted sill. Figure 19 shows the resulting positive / negative ratio / inclination $\underline{I}_{TV}$ graph. The residual curve's positive / negative ratio (see fig. 18) of about 16 was used; the apparent inclinations found from this graph corresponded to 148° to 151° for thicknesses of 800 to 50 feet respectively. At first, model curves were computed for a strike angle $\underline{\alpha}_{TV}$ of 90°, unit intensity, and depths of 100, 150, and 200 feet for these thicknesses and

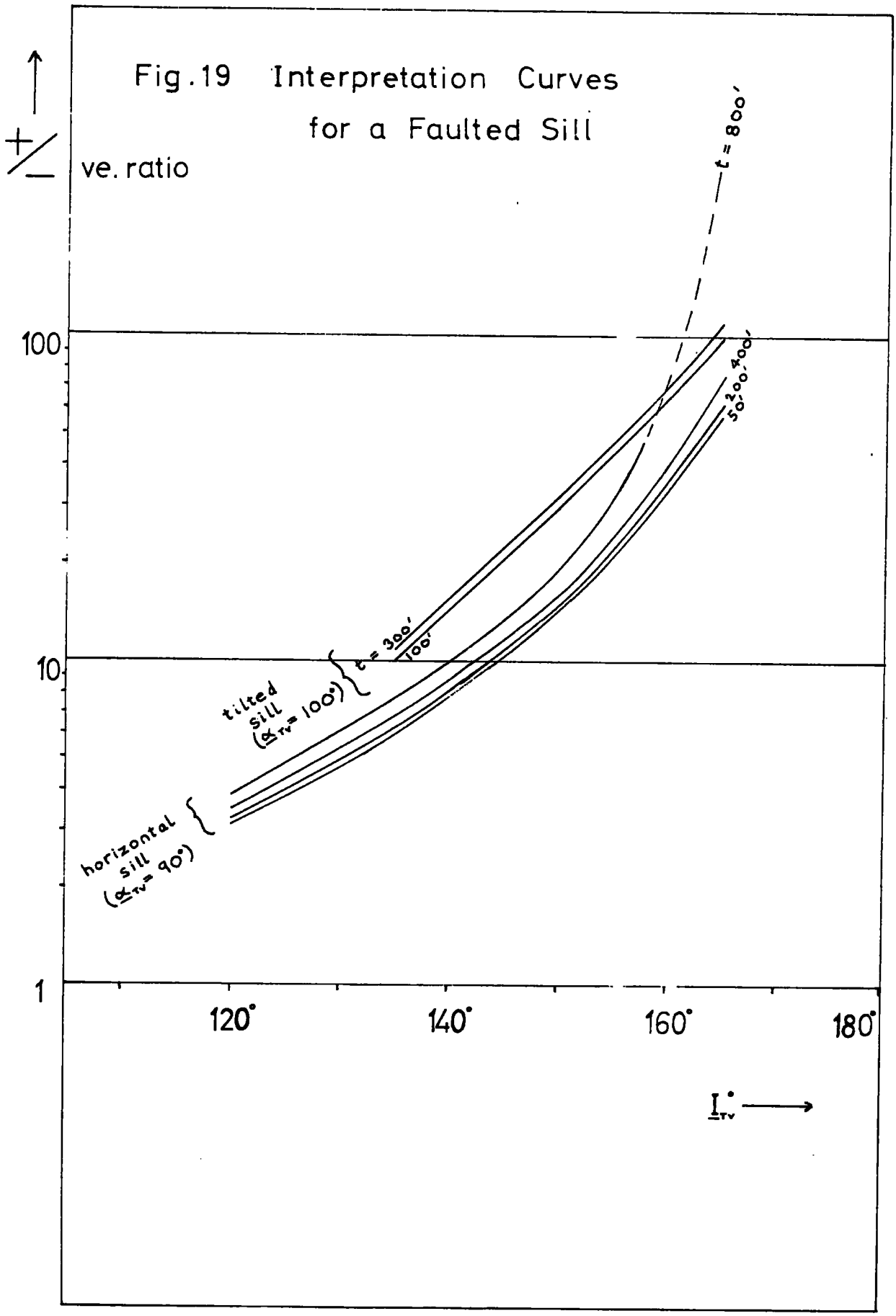
Fig.19 Interpretation Curves for a Faulted Sill
+/− ve. ratio
100
10
1
t = 800'
50, 200, 400'
t = 300'
100'
tilted sill (α_Tv = 100°)
horizontal sill (α_Tv = 90°)
120°
140°
160°
180°
I_Tv°

inclinations. But when these were scaled to the residual profile their negative portions did not agree in shape, and the values on the southern flanks diminished too slowly. Several remedies were possible however: by (a). diminishing the inclination $\underline{I}_{TV}$ slightly to about 146°; by (b). diminishing the strike angle α_{TV} to about 100°; or by (c). calculating for a tilted sill.
The ideas of (a) and (b) were used in the computation of further models shown in fig. 20, (corresponding interpretations of these will follow in the next paragraphs). When it was realised that the negatives of the above models were not of the correct shape, a new graph of ratios / inclinations was constructed for a tilted sill (fig. 19) using a strike angle of 100°. From fig. 18 the positive /negative ratio of about 16 corresponded to an apparent inclination $\underline{I}_{TV}$ of about 141°. Theoretically however, this new inclination demands that the strike angle should be further reduced to about 110° because the remanent component has been progressively lessened. The final profiles to be calculated for this thesis are shown in figure 21.

The observations and conclusions made from all the models for a horizontal and tilted sill are set out in their order of reasoning below.

(1). The curves are of similar shape to the residual curve.

(2). The apparent inclinations $\underline{I}_{TV}$ used must be reasonably accurate, to within about 15°, in order to produce the required amount of dip to the negative portion; this accuracy is further improved in the final curves. The value of the background anomaly is considered to be sufficiently accurate.

(3). The positive peaks diverge only slightly from the residual peak position.

(4). The negative and upper positive areas generally agree with those of the residual; the middle parts and to a lesser extent

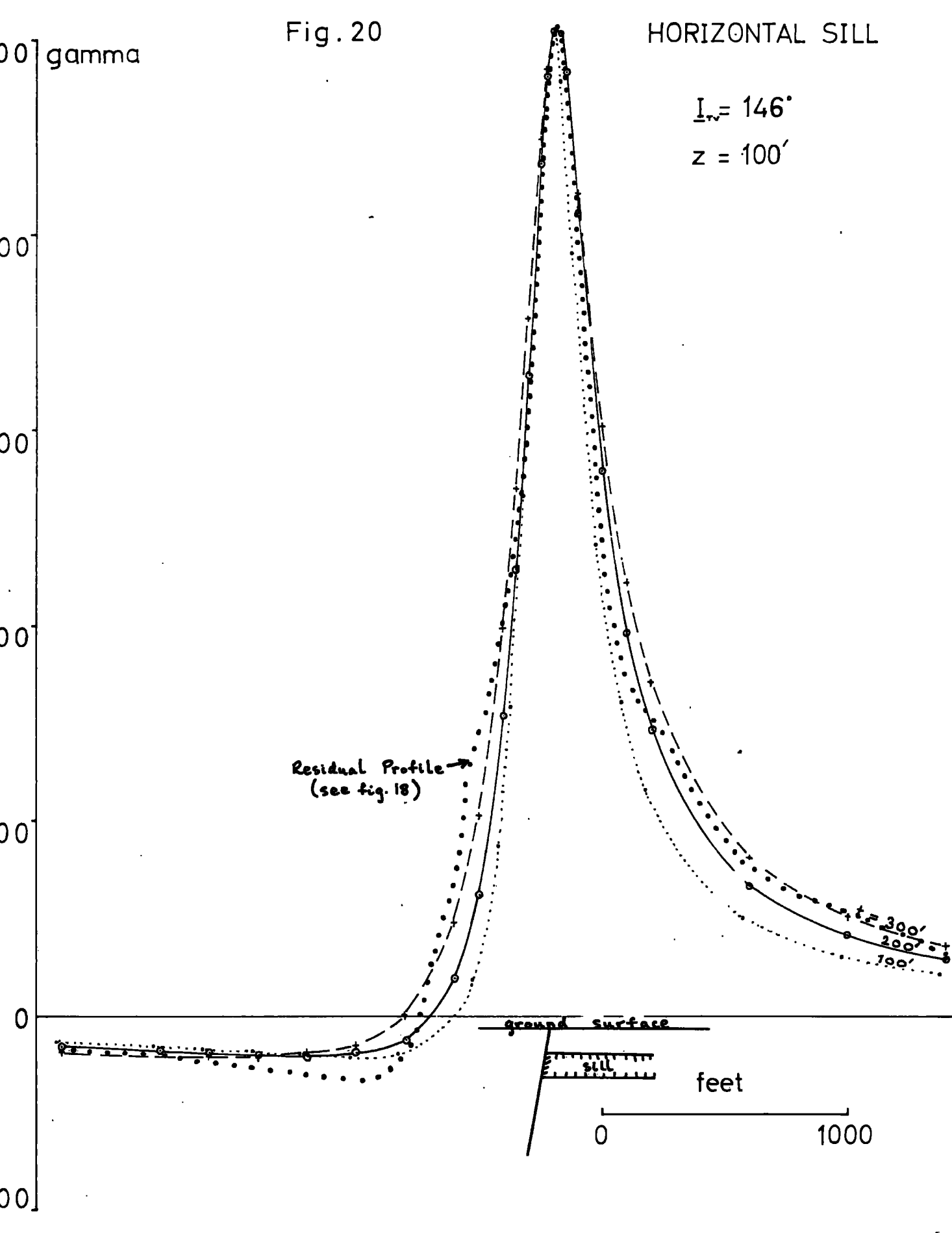
Fig. 20
HORIZONTAL SILL
gamma
I_{rv} = 146°
z = 100′
Residual Profile
(see fig. 18)
t = 300′
200′
100′
ground surface
sill
feet
0
1000

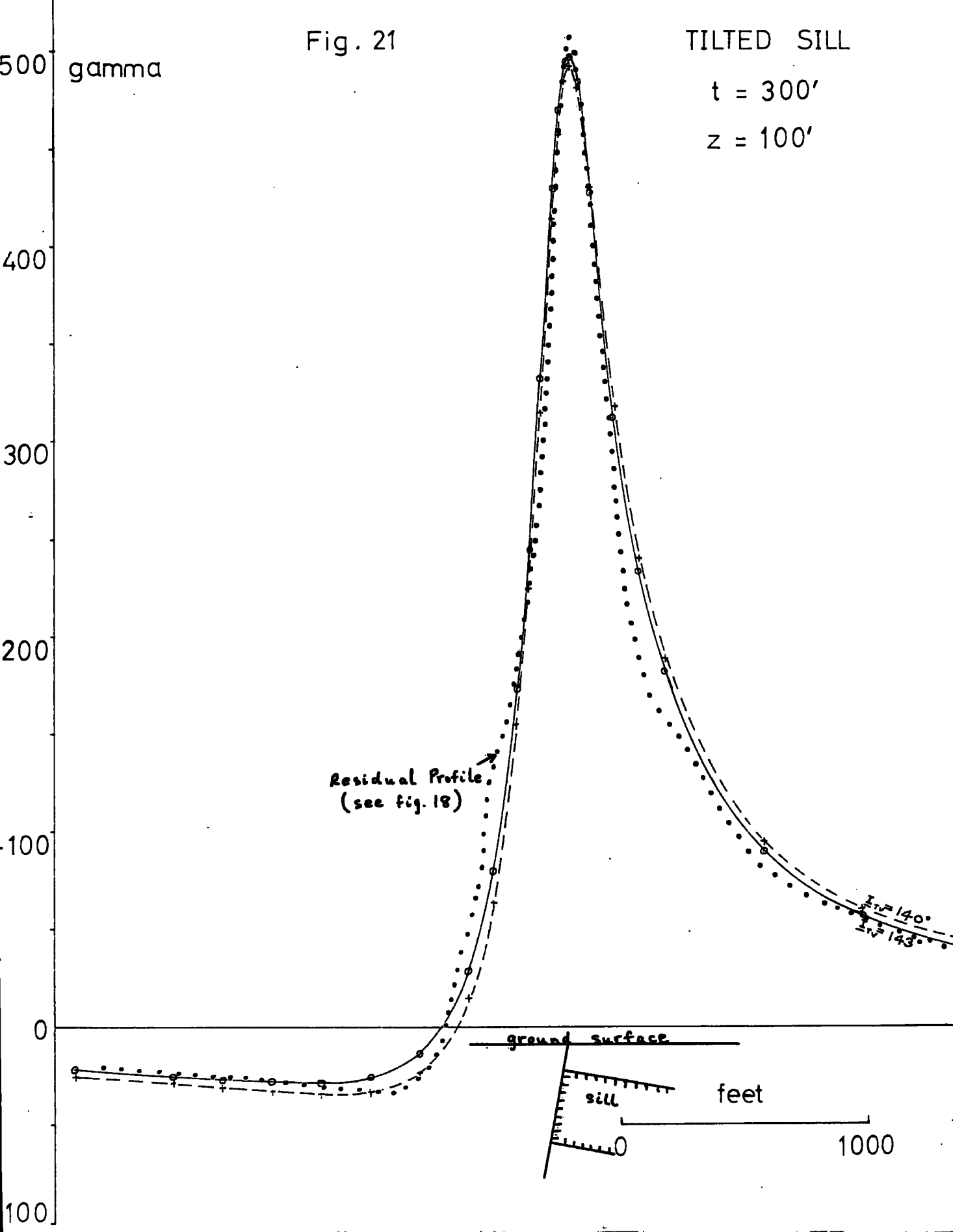
Fig. 21
TILTED SILL
t = 300'
z = 100'
gamma
500
400
300
200
100
0
100
Residual Profile
(see fig. 18)
I = 140°
I = 143°
ground surface
sill
feet
0
1000

the southern flanks are more difficult to fit.

(5). The negative portions are displaced northwards with increase of thickness but the positive peaks remain almost stationary; the negative portions also diverge with increase of depth.

(6). The thickness and depth are easily resolved in this problem because a). the positive peaks become rounded with increase of depth, and b). the depth is more known than the thickness.*

(7). It follows that the middle and lower portions of the residual curve suggest a considerable thickness of rock; the sharp positive peak suggests either a moderate or relatively shallow depth, or a high apparent intensity of magnetisation $\underline{J}_{TV}$.

(8). The models agree with the suggestions made in (7).

(9). For the negative portion the most suitable inclinations are those for $\underline{I}_{TV} = 140^{\circ}$ and 143° (fig. 21). This means that the remanent component is less than the average observed value of $\underline{J}_{rT} = 2.8 \times 10^{-3}$ cgs. (Creer and others, 1959).

(10). Since the apparent intensity $\underline{J}_{TV}$ is low, in order to obtain an anomaly of sufficient magnitude to fit the residual, either the thickness must be increased or the depth decreased.

(11). From (6) and (7), a). the depth is probably less than 100 feet.

b). the thickness is over 200 feet.

c). for a depth of 100 feet the thickness would be nearer 300 feet.

d). for a thickness of 300 feet, a depth of 100 feet, and an inclination of 140°, the factor required to scale the calculated profile to the residual, or the apparent intensity of magnetisation $\underline{J}_{TV}$, is approximately 2×10^{-3} cgs. units.

(12). The value of $\underline{J}_{TV}$ found in (11.d) can be checked from vector analysis. Using $\underline{J}_{iT} = 1$ (or 10^{-3}), $\underline{I}_{rT} = 170^{\circ}$, $\underline{I}_{iT} = 70^{\circ}$, $\underline{I}_{TV} = 140^{\circ}$, then $\underline{J}_{TV} = 2 \times 10^{-3}$ and $\underline{J}_{rT} \approx 1.9 \times 10^{-3}$. The angle of 170° for $\underline{I}_{rT}$ is well within the observed limits for the Whin Sill (refer to p. 33).

* i.e. it was known with reasonable certainty, from the geological evidence (interpolated from maps, boreholes, etc.) that the depth was not more than about 150 feet; the thickness was completely unknown.

The answers derived from the above physical analysis are a good approximation to the nature of the body causing the Coanwood anomaly. Uncertainties of the basement rocks prevent really accurate results, but the values given in the above sections should provide good approximations to the actual conditions. A faulted Whin Sill and basement can adequately explain the observed anomaly. There is no need to infer the presence of any other body such as a dyke. The Whin Sill is likely to thicken considerably in the Coanwood area, and to lie at a relatively shallow depth. Its inclination, declination, and intensity closely agree with those of Creer and others (1959).

Errors involved in deriving these results are mostly related to the basement rocks. The data used to compute the basement anomalies may not be sufficiently accurate. The value of the background field is always difficult to assess, but on the basis of the shape and inclination of the residual curve it is considered to be relatively accurate; similarly is the process by which it was evolved. In computing the effects of the sill the only errors likely to occur, and these are slight, are the uncertainty of the correct value of the apparent strike angle α_{TV} and in neglecting the effects of the downthrown side. Another effect is in calculating for a semi-infinite sill of uniform thickness, as it is most unlikely that the proposed thickening extends to great distances southwards. The time factor unfortunately prevented a continuation of this research into a really accurate determination of the dimensions and other physical data of the Whin Sill at Coanwood.

Having dealt at length with the Coanwood anomaly, and knowing the physical possibilities of the region, attention may now be diverted to the rest of the anomaly map. Boghead, section CD (fig. 6) suggests a similar picture to that of Coanwood. The sharp gradients up to the positive peak indicate

either a relatively shallow depth or a high intensity of magnetisation. On the other hand, the width of the central and lower portions of the curve suggests that at Boghead the Whin Sill is very thick. Evidence to support this suggestion is ample :

(a). The total size of the anomaly is greater than it is at Coanwood.

(b). The effects of a faulted basement are here less, owing to the progressive decrease of the throw.

(c). The angle of strike of the anomaly to the present meridian is less than at Coanwood, about 78°: it is suggested that the total size of the Boghead anomaly is less than it would be if the strike angle was nearer 90°.

Points (b) and (c) contribute to a relative increase in the total size of the residual anomaly (observed minus basement) of Boghead over that of Coanwood. Assuming a similar apparent intensity of magnetisation $\underline{J}_{TV}$, and a similar depth to those of Coanwood, this increase in size can only be attributed to a greater thickness of basic rock. (The depth to the sill on the south side of the fault must be considerably less than has hitherto been realised in order to cause such an anomaly). One difficulty in this interpretation however, is there is a negative trough immediately south of the positive peak. This may be explained in several ways :

(i). The apparent inclination $\underline{I}_{TV}$ may be different from that of Coanwood.

(ii). A natural slope may confine the Whin Sill on its southern side to a kind of trough : if the magnetisation is similar to that at Coanwood then negative poles would be induced on this face if the slope angle is relatively great.

(iii). Small faults may affect the Whin Sill just south of the

Stublick Fault - an alternative to (ii).

(iv). It may be necessary to assume the presence of another body such as a dyke.

All these points must now be studied more closely :

(i). When the effects of the basement are subtracted from the Boghead profile the northern negative trough will become almost non-existent, but the southern trough will be deepened. Bearing this in mind the profile should now be turned end for end, with the deepened negative trough on the north side. A striking similarity to the Coanwood profile is immediately noticed. This means that the apparent inclination $\underline{I}_{TV}$ would be directed upwards at maybe -130° to -170°. A consequence of such inclinations would be a tendency for the axis of the positive peak to diverge northwards. Such inclinations however, would be anomalous for the Whin Sill.

(ii). A wall or slope on the south side of the Stublick Fault may have confined the rock when molten within a kind of ' chamber '. If the inclination is similar to that of Coanwood, negative poles would be induced on this southern face resulting in a small positive anomaly and stronger negative anomaly. It is thought that this explanation may account for the small negative anomaly on the south side of the Coanwood profile, but here the southerly face may only be a gentle slope.

(iii). A small fault may occur south of and close to the Stublick Fault to affect the sill. Assuming the Coanwood inclination and a southerly throw, negative poles would be

induced along the fault plane in a manner similar to that of (iii) above. The result would be a small positive anomaly north of this fault and a larger negative anomaly to the south of it. The fault should be sufficiently close to the Stublick Fault so that the main positive anomaly would adsorb the smaller one without causing a bump on the profile.

(iv). A profile similar to that of Boghead can be obtained by assuming a polarisation in a similar direction to that of the present field, across a dyke having its lower end at only moderate depth. Two important points about dykes, and referred to earlier in this chapter, apply here. If the apparent inclination $\underline{I}_{TV}$ departs either way from +70° then the positive peak will diverge from the Stublick Fault plane. In order to coincide with the observed anomaly the inclination is thus limited to about +70° to +110° for a vertical dyke. Also, the thickness of the dyke must be very limited in order for the positive peak to coincide with the fault plane.

Here the problem of the Boghead anomaly will be left until the geological discussion. On the anomaly map there are several other interesting features to be accounted for. Some of these are associated with the positive belt (see Plate 1). From a maximum value at Coanwood the positive anomaly diminishes rapidly near section AB, but more gradually further east. The decrease is probably due to an increase in depth and decrease in thickness of the Whin Sill. Near grid reference line 70 (N-S) there is a sudden widening of the positive anomaly and an increase in amplitude. But the anomalies north and south of it continue their eastward decrease, unaffected by this change. The following points have been made:

(a). From the shape of the anomaly there does not appear to be a decrease of the depth to the Whin Sill.

(b). The increase in anomaly width suggests a sudden thickening

of the sill.

(c). The unchanged anomalies to the south and north are evidence against (b). It is possible that another body may be present at depth, perhaps a dyke. This body may have normal or vertical polarisation and it may be relatively thick.

(d). The presence of a dyke has been proved in adjacent coal mines (Trotter and Hollingworth, 1932, and personal communication, 1960).

Following grid line 71 there is a very flat field south of the positive ridge. If the interpretation of (iii) above was correct, this could mean that a southerly wall carrying negative poles no longer influences the general field. In other words, the Whin Sill here may be of uniform thickness, and the flat field a true representation of basement faulting plus the faulting of a uniformly thick sill. The sudden end of the positive ridge between lines 71 and 72 is probably caused by a considerable reduction in the thickness of the sill. The reason for the transgression of the central axis here north of the fault is not yet known. The anomalies west of Coanwood should be interpreted with caution, as pointed out in Chapter III. It does appear certain however, that much of the Coanwood positive anomaly ends near grid line 68, and that a smaller positive anomaly persists west of it, along the fault line. In spite of the confusion of contours west of Coanwood, the effects of the basement can still be isolated: north of the Stublick Fault persists the broad negative anomaly. The field in the extreme south of this area compares favourably with the flat field along line 71; it is likewise probable that the anomalies are entirely due to basement faulting and faulting of a uniformly thick sill. The eastward extension of the Boghead

anomaly appears to be limited between lines 74 and 75. Further east it is assumed that the Whin Sill again resumes its uniform relatively small thickness.

Although the physical interpretation could be extended through many more pages, space must be left for a discussion of the Haltwhistle anomalies from a geological viewpoint. Emphasis is placed upon the origin of the disturbing bodies.

(d). Geological Aspects of the Interpretation.

It has been stated in Chapter I that the only known rocks in the area capable of producing such anomalies as those near Haltwhistle belonged to the Whin Sill Group. The proposal of a dyke in 1958 within the Stublick Fault zone, possibly as a major feeder to the Whin Sill, was then a very attractive suggestion. Geologically however, this would have been rather difficult to correlate with the structures of the area, especially when the proposed width was about 600 feet. It would also have produced tremendous pressures within the fault zone owing to such a massive body, (Anderson, 1951). The new palaeo-magnetic evidence for the Whin Sill however, prevented these problems from arising.

The great differences in form and texture of the Whin Sill north and south of the fault, which have been described in Chapter I, are evidence favouring the proposal of thickened pockets of basic rock. The reasons for their occurrence are not yet clear, but perhaps they can be explained by pressure effects. At the time of intrusion the thickness of overlying sediments north of the fault was apparently much greater than that to the south. On the Alston Block there was perhaps a sudden release of pressure on the mobile magma, such as might have occurred

when it approached a zone of weakness, e.g. the Stublick Fault area. This could have resulted in the expulsion of volatiles, a slowing down of its movement, and a gradual accummulation of a considerable thickness of magma near to the fault zone. Any remaining volatiles however, may have helped to keep some of the magma mobile, resulting in the northward extension of the sill into the Northumbrian Trough. The presence of thick overlying sediments and the diminished reserves of magma would both help to restrict the sill to only thin sheets in this trough. The feeding sources of this rock still remain a mystery, but further investigations may yet reveal their presence. The dyke discovered along the fault zone in the coal workings (Trotter and Hollingworth, 1932) can certainly never be regarded as a major feeder owing to the small size of the anomaly. As pointed out above, the cause of the Boghead anomaly is considerably more difficult to explain than that of Coanwood, and the possibility of dykes there are not yet ruled out, in spite of the many convincing arguments to the contrary. Another point is that in the area of low anomalies, between the two Coanwood and Boghead anomalies, the Whin Sill may be present but not faulted.

It is not fully understood why the proposed areas of thickened sill occur where the fault line curves northwards in gentle arcs. Another structural problem is to relate the thickened sill to the important fault junction at Coanwood (see fig. 2). In 1958 evidence for the presence of local thickening appeared in somewhat unusual form, very close to this fault junction. Several years ago a severe thunderstorm broke out over the area. Lightning was actually observed to strike the same field in which the highest magnetic anomalies were recorded, at a distance of less than twenty yards from them and the fault junction. The earth was torn up resulting in a large hole several feet deep, but this has since been filled in. It should be noted

that it is rare for lightning to strike a bare field. However, a study of the relations of lightning strikes to magnetic rocks, interesting though it should be, is another problem which can not be considered here.

The conclusions to the work and results of this thesis are given in the next chapter, ending in a summary of the possibilities of future field work and research in and around the Haltwhistle region.

CHAPTER VI

Conclusions, Future Work, and Acknowledgements

The following topics have been examined and completed during the course of this research work:

(i). A magnetic survey has been carried out in detail over part of the Stublick Fault line near Haltwhistle. A belt of major positive magnetic anomalies was discovered.

(ii). A comparison of these new anomalies was made with the anomaly over the Hett Dyke. The dyke hypothesis for explaining the Haltwhistle anomalies had to be rejected almost completely.

(iii). The magnetic anomalies resulting from the faulting of the Whin Sill by the Stublick Fault have been calculated on a computer using new palaeomagnetic data on polarisation directions.

(iv). The effects of faulting the basement rocks have been calculated. They have been found to affect the lateral parts of the observed anomalies.

(v). Most of the observed positive anomalies, particularly in the west, are adequately explained by the faulting of a locally thickened Whin Sill. The possibility of small dykes acting as feeders to the sill along the fault plane still remains, especially in the east.

The main points of magnetic interpretation which have been brought out in this work are listed below.

(1). A complete and comprehensive magnetic interpretation programme for use on a computer has been devised and successfully proved, in which magnetic profiles can be obtained for any two-dimensional body. Any parameter may be chosen and all known magnetic data can be included in the programme.

(2). Interpretation of the anomalies shows the importance of remanent magnetism. For a complete interpretation it is usually necessary to know the Koenigsberger Ratio and the directions of both magnetising fields.

(3). Detailed analyses of magnetic curves have produced valuable information on interpretation techniques. Methods are being devised whereby it will be possible to obtain all information from a single magnetic curve.

(4). The analyses of magnetic anomalies caused by simple bodies is relatively easy and rapid, but as in the Haltwhistle case where more complex structures and two or more bodies occur, the interpretation becomes more difficult.

There remains much work to be done in and around the Haltwhistle region, and in the research into interpretation procedures. A summary of the future work provides a suitable conclusion to this thesis, which has been compiled specially for the M.Sc. degree.

(a). Detailed magnetic profiles should be obtained across the areas east of the present survey limits and across the Stublick Fault zone. Perhaps new similar anomalies may be found which may contribute further valuable information to our knowledge of that widespread basic rock, the Whin Sill of Northern England. Valuable information may also be obtained from detailed gravity traverses performed in conjunction with the magnetic surveys.

(b). Magnetic profiles should be taken over other areas where the Whin Sill is known to be faulted, and where all depths and dimensions are accurately known. Palaeomagnetic measurements must also be made in these areas.

(c). Vertical and total field magnetic surveys should be done systematically over known Hercynian and Tertiary dykes, followed by a tabulation of their properties and dimensions and

analyses of their results.

(d). i). A magnetic programme can be devised in which all computed profiles are reduced to certain standards and then compared directly.

ii). As a development of (i) it may become possible to insert a complete field profile, corrected for the background field, directly into a computer in which it is compared with standardised profiles and which are automatically rejected until the closest possible fit is found.

(However, since this thesis has been compiled it has been brought to the writer's notice that some of the suggestions made in (d) above have already been successfully carried out as research for a higher degree.)

(e). The methods in (d-i, ii) are regarded as procedures for solving a field anomaly indirectly, by trial and error. The direct interpretation however, of a field anomaly results in detailed measurements and analyses of various parts of the observed profile, and references to special tables and graphs (Werner, 1949, pp. 5, 6). It is therefore necessary for a series of tables, graphs, and possibly nomograms to be constructed for many different models having varying depths-widths, dips, and present and remanent magnetic field data. The time taken to solve a field profile using these procedures would compare very favourably with those described in (d-i and ii).

Acknowledgements:—

The writer wishes to express his gratitude to Dr. M. H. P. Bott for his advice and inspiration throughout the work, and who originally suggested the survey. Thanks are also given to the following : the Geology Department of the Durham Colleges in the University of Durham, for the loan of the

magnetometer; Father Lawrence of Stonyhurst College, who kindly lent photographic records of the daily variation; the Superintendent of Eskdalemuir Observatory, who supplied daily variation data; the people of Hamilton Publications (Burnley) Ltd., who bound this thesis; Mr. A. R. Smith, who kindly lent his motor-car for use in some of the field work; and the farmers and miners of the Featherstone area, for their helpful co-operation. The Department of Scientific and Industrial Research provided a research grant for maintenance while at Durham.

List of References.

ANDERSON, E. M. 1951. The dynamics of faulting and dyke formation, with applications to Britain. Oliver and Boyd, London. 2nd. edn.

BOTT, M. H. P. and D. MASSON-SMITH. 1957. Interpretation of a vertical field magnetic survey in North-East England. Quart. J. geol. Soc. Lond. 113, 119-29.

CREER, K. M., E. IRVING, A. E. M. NAIRN, & S. K. RUNCORN. 1959. The palaeomagnetism of the great Whin Sill of Northern England. Geophys. J. 2.

DUNHAM, K. C. 1948. Geology of the Northern Pennine orefield. Volume I. Tyne to Stainmore. Mem. geol. Surv. U. K.

EWING, W. M. and F. PRESS. 1952. Trans. Amer. geophys. Un. 33, 3.

HALLIMOND, A. F. and A. J. BUTLER. 1949. Miner. Mag. 80, 265.

HEILAND, C. A. 1940. Geophysical exploration. Prentice-Hall, N. York.

HOLMES, A. and H. F. HARWOOD. 1928. The age and composition of the Whin Sill and the related dykes of the North of England. Miner. Mag. 21, 493-542.

JAKOSKY, J. J. 1950. Exploration Geophysics. Trija, Los Angeles.

MARR, J. E. 1921. The rigidity of North-West Yorkshire. Naturalist, Lond. 63-72.

* BOTT, M.H.P. and D. MASSON-SMITH. 1957. The geological interpretation of a gravity survey of the Alston Block and the Durham Coalfield. Quart. J. geol. Soc. Lond. 113, 93-117.

MATUYAMA & HIGASINAKA. 1930. (see Heiland, 1940).

NETTLETON, L. L. 1942. Gravity and magnetic calculations. Geophysics. 7, 293-310.

RAYNER, D. H. 1953. The lower Carboniferous rocks in the North of England: a review. Proc. Yorks. geol. Soc. 28, 231-315.

SHOTTON, F. W. 1935. The stratigraphy and tectonics of the Cross Fell inlier. Quart. J. geol. Soc. Lond. 91, 639-704.

TALWANI, M., J. L. WORZEL, & M. LANDISMAN. 1959. Rapid gravity computations for 2-d bodies. J. geophys. Res. 64, 49-59.

TEALL, J. J. H. 1884. Petrological notes on some North of England dykes. Quart. J. geol. Soc. Lond. xl, 211-12.

TOMKEIEFF, S. I. 1929. A contribution to the petrology of the Whin Sill. Miner. Mag. 22, 100-20.

TOPLEY, W. and G. A. LEBOUR. 1877. On the intrusive character of the Whin Sill of Northumberland. Quart. J. geol. Soc. Lond. 33, 406.

TROTTER, F. M. 1929. The Tertiary uplift and the resultant drainage of the Alston Block and adjacent areas. Proc. Yorks. geol. Soc. 21, 161-80.

——— and S. E. HOLLINGWORTH. 1928. The Alston Block. Geol. Mag. 65, 433-48.

——— and S. E. HOLLINGWORTH. 1932. The geology of the Brampton district. Mem. geol. Surv. U. K.

TÖRNQVIST, G. 1952. Om den matematisk - geologiska tolkningen av magnetiska anomalier. Acta Acad. Åbo, Mat. Phys. XVIII, 2.

VERSEY, H. C. 1927. Post-Carboniferous movements in the Northumbrian fault block. Proc. Yorks. geol. Soc. 21, 1-16.

WALKER, G. W. 1919. The magnetic re-survey of the British Isles for the epoch Jan. 1, 1915. Phil. Trans. 219A, 1-72.

WERNER, S. 1949. Interpretation of magnetic anomalies at sheet-like bodies. Sverig. geol. Unders. Afh. Arsbok 43 (1949), no. 6.

WOOLACOTT, D. 1923. On a boring at Roddymoor Colliery, near Crook, Co. Durham. Geol. Mag. 60, 50-62.

DN

MAGNETIC ANOMALIES

Appendix 2 (c) : Specimen of Coded Programme.

XST YST Z H F = T

Main Programme (Part 1)

```
JI=0
*
STOP                    v48 49 50 51 52 53 54 55 56
v48=TAPE***.        ——— αLT, ILT, X1, Z1, X2, Z2, ITV, αTV, ITV
v44=3.14159265/180  ——— π/180
v43=3.14159265/2    ——— π/2
v49=v49Xv44         ——— ILT converted to radians
v48=v48Xv44         ——— αLT      "       "       "
v39=COSv49          ——— cos ILT
v49=SINv49          ——— sin ILT
v38=SINv48          ——— sin αLT
v39=v39Xv38         ——— sin αLT cos ILT
n1=0
n2=0

1)v2=v(53+n1)-v(51+n1)  ——— Z2 - Z1
→2,v2>0
v3=v(50+n1)             ——— X1
v(50+n1)=v(52+n1)       ——— X1 = X2
v(52+n1)=v3             ——— X2
v3=v(51+n1)             ——— Z1
v(51+n1)=v(53+n1)       ——— Z1 = Z2
v(53+n1)=v3             ——— Z2
v(54+n1)=-v(54+n1)      ——— ITV = -ITV
v2=-v2                  ——— -(Z2-Z1)

2)v(55+n1)=v(55+n1)Xv44 ——— αTV converted to radians
v(56+n1)=v(56+n1)Xv44   ——— ITV      "       "       "
v46=SINv(55+n1)         ——— sin αTV
v45=SINv(56+n1)         ——— sin ITV
v42=COSv(56+n1)         ——— cos ITV
v42=v42Xv46             ——— sin αTV cos ITV
v(55+n1)=v(54+n1)Xv45   ——— ITV sin ITV = IZV
v(54+n1)=v(54+n1)Xv42   ——— ITV sin αTV cos ITV = IHV
v4=v2Xv2                ——— (Z2-Z1)²
v5=v(50+n1)-v(52+n1)    ——— X1 - X2
v6=v5Xv5                ——— (X1 - X2)²
v7=v6+v4                ——— (X1 = X2)² + (Z2 - Z1)²
v7=**SQRTv7             ——— square root
v8=v2/v7                ——— Z2 - Z1 / square root = sin i
v(500+n2)=v8            ——— sin i stored
v9=v5/v7                ——— X1 - X2 / square root = -cos i
v(501+n2)=v9            ——— -cos i stored
n1=n1+7
n2=n2+2
→1,v(50+n1)≠0
STOP

***3)v40=TAPE2          ——— XST, YST
n1=0
n2=0
v0=0
v1=0

**4)v10=v(50+n1)-v40    ——— X1 - XST
v11=v10Xv10
v12=v(51+n1)-v41        ——— Z1 - YST
v13=v13+v11             ——— (X1 - XST)² + (Z1 - YST)²
→5,v13≠0
v13=***1

5)v13=SQRTv13           ——— r1
v14=v(52+n1)-v40        ——— X2 - XST
v15=v14Xv14
v16=v(53+n1)-v41        ——— Z2 - YST
v17=v15Xv16
v17=v17+v15             ——— (Z2 - YST) + (X2 - XST)
→6,v17≠0
v17=***1

6)v17=SQRTv17           ——— r2
v17=v17/v13
v17=LOGv17
v18=v17Xv(500+n2)       ——— sin i loge r2/r1
v19=v17Xv(501+n2)       ——— cos i loge r2/r1
→7,v12=0
v20=v10/v12
v20=ARCTANv20           ——— tan⁻¹ (X2 - XST)/(Z1 - YST)
→8
*
7)v20=v43               ——— π/2
→8,v10>0
v20=-v20

8)v20=v43-v20           ——— π/2 - θ1 = φ1
→9,v16=0
v21=v14/v16
v21=ARCTANv21           ——— tan⁻¹ (X2 - XST)/(Z2 - YST)
→10

9)v21=v43               ——— π/2
→10,v14>0
v21=-v21

10)v21=v43-v21          ——— π/2 - θ2 = φ2
v21=v21-v20
v22=v21Xv(500+n2)       ——— sin i (φ2 - φ1)
v23=v21Xv(501+n2)       ——— cos i (φ2 - φ1)
v24=v23+v18
v25=v24Xv(54+n1)        ——— IHV.[cos i (φ2-φ1) + (sin i loge r2/r1)]
v26=v22-v19
v27=v26Xv(55+n1)        ——— IZV.[sin i (φ2-φ1) - (cos i loge r2/r1)]
v28=v25-v27
v29=v(500+n2)**X2
v30=v28Xv29
v30=v30X100000          ——— convert to gammas = ΔZ
v0=v0+v30               ——— store ΔZ = ΔZ1 + ΔZ2 + ..... = ΔZTOTAL
v31=v26Xv(54+n1)
v32=v24Xv(55+n1)
v33=v32+v31
v33=v33Xv29
v33=v33X100000          ——— ΔH
v1=v1+v33               ——— store ΔH = ΔH1 + ΔH2 + ..... = ΔHTOTAL
n1=n1+7
n2=n2+2
→4,v(50+n1)≠0

PRINTv40,3201
PRINTv41,4201
PRINTv0,4181
PRINTv1,4161
v34=v1Xv39              ——— ΔHTOTAL . cos ILT sin αLT
v35=v0Xv49              ——— ΔZTOTAL . sin ILT
v36=v34+v35             ——— ΔTTOTAL
PRINTv36,4161
→3
(→0)
```

Appendix 2 (a)

Flow diagram of programme.

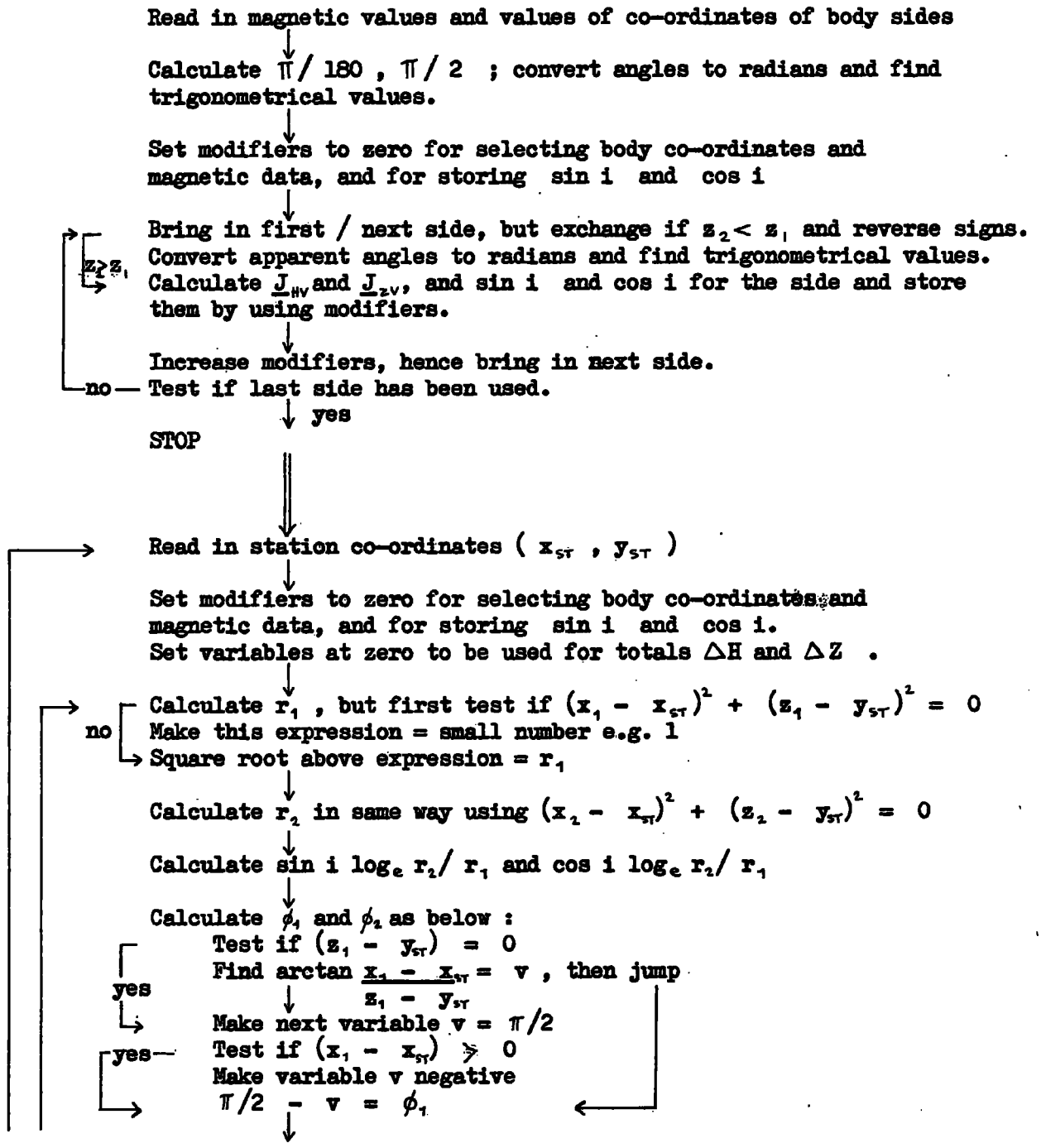

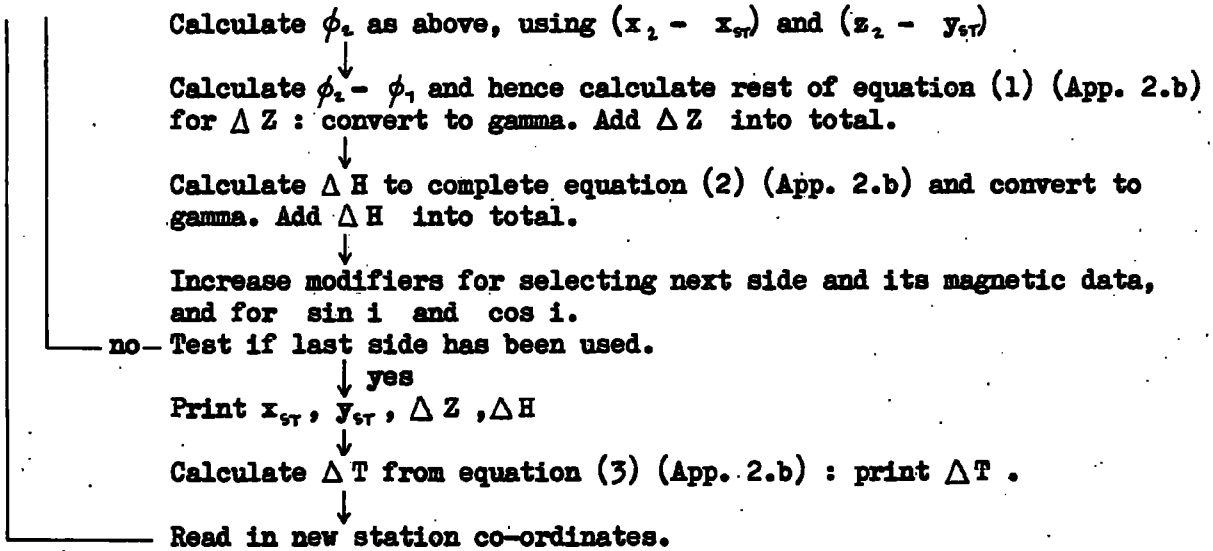
Calculate ϕ_2 as above, using $(x_2 - x_{ST})$ and $(z_2 - y_{ST})$
Calculate $\phi_2 - \phi_1$ and hence calculate rest of equation (1) (App. 2.b) for ΔZ : convert to gamma. Add ΔZ into total.
Calculate ΔH to complete equation (2) (App. 2.b) and convert to gamma. Add ΔH into total.
Increase modifiers for selecting next side and its magnetic data, and for sin i and cos i.
no
Test if last side has been used.
yes
Print x_{ST}, y_{ST}, ΔZ, ΔH
Calculate ΔT from equation (3) (App. 2.b) : print ΔT .
Read in new station co-ordinates.

Appendix 2 (d: i)

Specimen of input data for the computer, used to obtain the results shown in App. 2 (d: ii) for a faulted and tilted sill ; STR = strike angle α_{TV} and I = I_{TV}. (see Chapter IV for an explanation of the printing sequence).

```
N
STR. = 110  I = 143

JI.2
(→0)

+97 +70
+13000 +100 +0 +2378 +1 +110 +143
+120 +2678 +13120 +400 +1 +110 +143
+13120 +400 +13000 +100 +1 +110 +143
+0 +0 +0
L
*********
N
I = 140

JI.2
(→0)

+97 +70
+13000 +100 +0 +2378 +1 +110 +140
+120 +2678 +13120 +400 +1 +110 +140
+13120 +400 +13000 +100 +1 +110 +140
+0 +0 +0
L
*********
```

Appendix 2 (d: ii)

Specimen of results from the data given in App. 2 (d: i), and used to plot the profiles shown in figure 21. Scaling factor = $\underline{J}_{TV} = 1.9 - 2.0 \times 10^{-3}$

4096 AUTOCODE MK. 4

19/8/60---14
MAGNETIC ANOMALIES

XST	YST	Z	H	F = T
STR. = 110 I = 143				
+11400.0	+0.0	+21149.3	+29392.0	+29851.5
+11800.0	+0.0	+29509.4	+36896.7	+40255.1
+12200.0	+0.0	+46720.6	+48944.0	+60518.1
+12600.0	+0.0	+95557.4	+66651.3	+112420.7
+12700.0	+0.0	+122774.9	+68728.6	+138702.0
+12800.0	+0.0	+164179.6	+62352.3	+175445.1
+12900.0	+0.0	+224844.6	+26489.9	+220277.4
+12950.0	+0.0	+254530.2	-19029.1	+232720.3
+12975.0	+0.0	+261970.1	-51158.4	+228804.6
+13000.0	+0.0	+259831.8	-86686.3	+214734.6
+13025.0	+0.0	+246967.2	-120526.6	+191158.0
+13050.0	+0.0	+225838.2	-148049.0	+161960.2
+13100.0	+0.0	+174791.5	-179442.2	+103334.8
+13150.0	+0.0	+128055.1	-187483.8	+56687.2
+13200.0	+0.0	+90902.9	-183277.4	+23203.4
+13300.0	+0.0	+41617.8	-161389.1	-15679.0
+13400.0	+0.0	+14615.1	-137007.4	-32776.3
+13600.0	+0.0	-7709.8	-99087.5	-40882.1
+13800.0	+0.0	-13970.6	-75140.1	-38635.9
+14000.0	+0.0	-15335.3	-59723.8	-34684.9
+14200.0	+0.0	-15112.9	-49247.2	-30919.5
+14400.0	+0.0	-14379.1	-41756.0	-27686.8
+14600.0	+0.0	-13513.0	-36169.2	-24976.5
+15000.0	+0.0	-11851.3	-28439.5	-20790.9
I = 140				
+11400.0	+0.0	+22749.6	+28321.2	+30991.8
+11800.0	+0.0	+31523.7	+35395.2	+41638.2
+12200.0	+0.0	+49406.3	+46549.6	+62228.9
+12600.0	+0.0	+99272.4	+61693.5	+114228.7
+12700.0	+0.0	+126649.6	+62328.1	+140170.3
+12800.0	+0.0	+167790.4	+53739.8	+175914.4
+12900.0	+0.0	+226659.2	+14588.5	+217942.4
+12950.0	+0.0	+253979.4	-32590.5	+227599.0
+12975.0	+0.0	+259725.3	-65173.4	+221937.5
+13000.0	+0.0	+255695.0	-100651.8	+206106.3
+13025.0	+0.0	+241008.7	-133869.7	+181029.2
+13050.0	+0.0	+218378.8	-160319.1	+150785.3
+13100.0	+0.0	+165571.3	-189056.1	+91407.1
+13150.0	+0.0	+118323.0	-194628.4	+45116.6
+13200.0	+0.0	+81327.1	-188440.0	+12452.6
+13300.0	+0.0	+33116.0	-163892.9	-24518.0
+13400.0	+0.0	+7360.3	-138032.0	-39941.4
+13600.0	+0.0	-12989.7	-98857.0	-45765.4
+13800.0	+0.0	-17989.2	-74533.6	-42206.3
+14000.0	+0.0	-18537.0	-59016.9	-37453.6
+14200.0	+0.0	-17757.5	-48533.2	-33162.2
+14400.0	+0.0	-16624.2	-41067.4	-29562.8
+14600.0	+0.0	-15459.7	-35516.5	-26584.1
+15000.0	+0.0	-13384.2	-27861.1	-22035.0

Appendix 2 (b)

Magnetic formulae actually used in programme (see Appendices 2-a,c); in modified form they are shown in the text in equations (10) - (12).

$$\Delta H = 2 \sin i \left\{ \underline{J}_{HV} \left[\sin i \, (\phi_2 - \phi_1) - \cos i \log_e r_2 / r_1 \right] + \underline{J}_{ZV} \left[\sin i \log_e r_2 / r_1 + \cos i \, (\phi_2 - \phi_1) \right] \right\} \text{ - - - - - - - - (1)}$$

$$\Delta Z = 2 \sin i \left\{ \underline{J}_{HV} \left[\sin i \log_e r_2 / r_1 + \cos i \, (\phi_2 - \phi_1) \right] - \underline{J}_{ZV} \left[\sin i \, (\phi_2 - \phi_1) - \cos i \log_e r_2 / r_1 \right] \right\} \text{ - - - - - - - - (2)}$$

$$\Delta T = \Delta H \cos I_{iT} \sin \alpha_{iT} + \Delta Z \sin I_{iT} \text{ - - - - - - - - - - - - - - - - (3)}$$

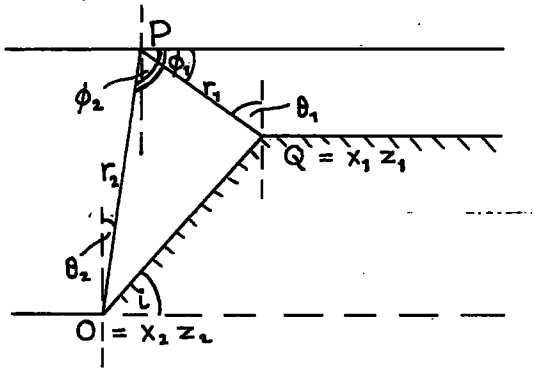

P is the station point at the surface, with co-ordinates x_{ST}, y_{ST}.

Q and O are body points x_1 z_1 and x_2 z_2 respectively.

Here, $\phi_1 = 90 - \theta_1 = \pi/2 - \theta_1$

$$= \pi/2 - \text{ARCTAN} \frac{x_1 - x_{ST}}{z_1 - y_{ST}}$$

If ARCTAN $\frac{x_1 - x_{ST}}{z_1 - y_{ST}}$ is negative, make this expression negative in programme, i.e. ϕ_1 will then be equal to $\pi/2$ + ARCTAN $\frac{x_1 - x_{ST}}{z_1 - y_{ST}}$

Similarly with ϕ_2.

$r_1 = \sqrt{(x_1 - x_{ST})^2 + (z_1 - y_{ST})^2}$: r_1 must not equal zero ; similarly with r_2. Therefore make r_1 and r_2 = a small number at least, e. g. 1 .

From the above figure, $\sin i = \frac{z_2 - z_1}{\sqrt{(z_2 - z_1)^2 + (x_1 - x_2)^2}}$

and $\cos i = \frac{x_1 - x_2}{\sqrt{(z_2 - z_1)^2 + (x_1 - x_2)^2}}$

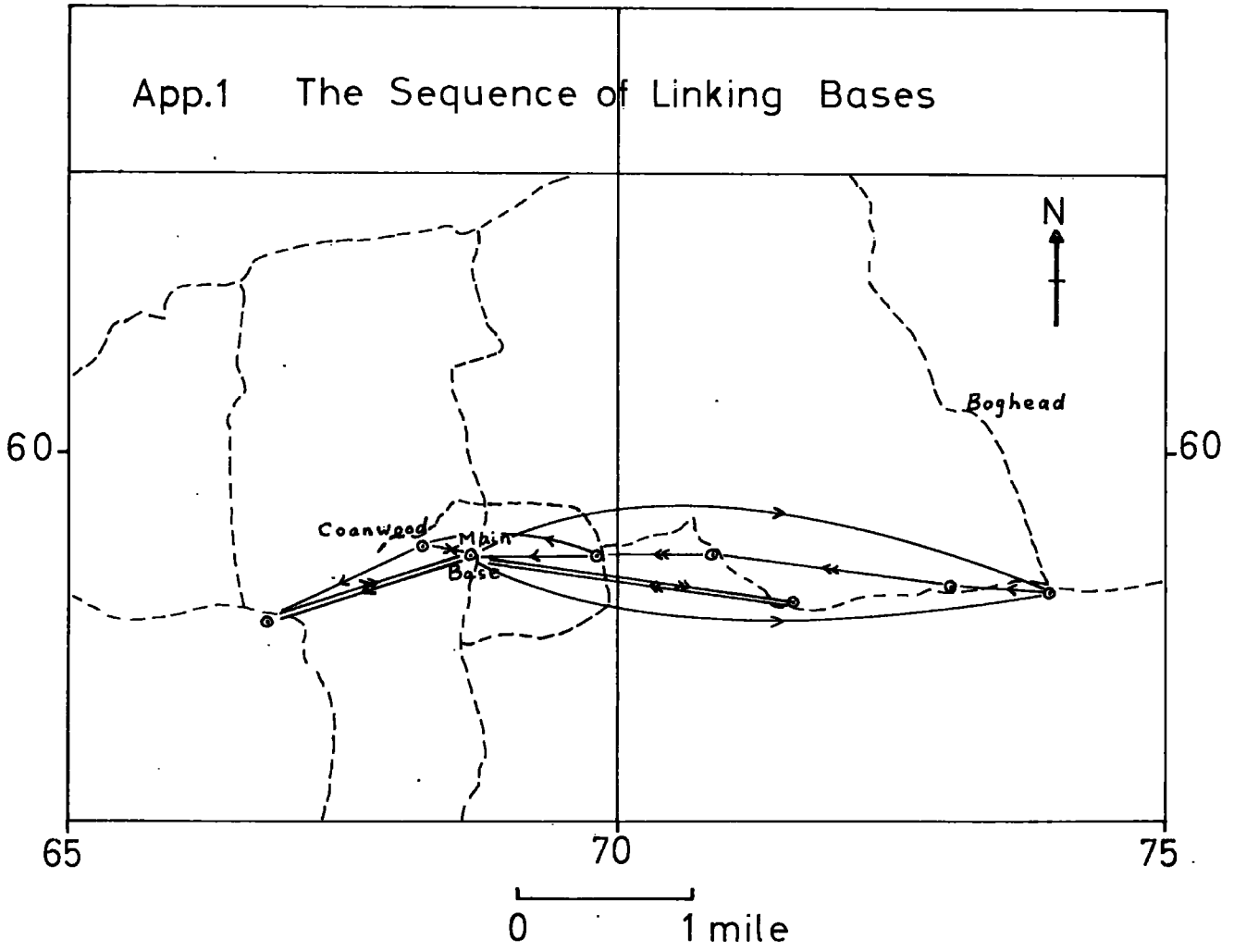
App.1 The Sequence of Linking Bases
N
Boghead
60
60
Coanwood
Main
Base
65
70
75
0
1 mile

PLATE 1

VERTICAL FIELD MAGNETIC ANOMALIES OVER PART OF THE STUBLICK FAULT